

**DESIGN, FABRICATION AND STUDY OF THE SINGLE ROTOR VTOL
SPHERICAL UAV**

A PROJECT REPORT

Submitted to

SRM UNIVERSITY

by

**KRISHTI DAS - 1191210122
SIDDHARTH DEORE - 1191210153**

in partial fulfilment for the award of the degree

of

BACHELOR OF TECHNOLOGY

IN

AEROSPACE ENGINEERING



DEPARTMENT OF AEROSPACE ENGINEERING

SRM UNIVERSITY

**KATTANKULATHUR- 603203,
CHENNAI, INDIA**

APRIL/MAY 2016

ACKNOWLEDGEMENT

On the very outset of this report, we would like to extend our sincere and heartfelt obligation towards all the personages who have helped us in this endeavor. Without their active guidance, help, cooperation and encouragement, we could not have made headway in the project.

First and foremost, we would like to express our sincere gratitude to our guides, Dr. Ramesh Kandadai and Mr. Umar Rizwan. we are privileged to experience a sustained enthusiastic interest from them which fuelled our thoughts to think broad and out of the box and explore .We would also like to thank our Head of the department, Dr. R. Vasudevan for his encouragement and guidance in right direction. We would also like to thank RPT Lab, Mechanical Department for helping us immeasurably in fabrication of our model.

We are indebted to a number of friends and well-wishers who have extended their cooperation and help in the preparation of the project. Last but not the least, we are deeply indebted to our parents for their support and their patient guidance.

CERTIFICATE

This is to certify that the project report entitled "**DESIGN, FABRICATION AND STUDY OF THE SINGLE ROTOR VTOL SPHERICAL UAV**" submitted by **SIDDHARTH DEORE** and **KRISHTI DAS** to the SRM University, Kattankulathur, in partial fulfilment for the award of Degree of Bachelor of Technology in Aerospace Engineering is a bonafide record of the project work carried out by them under my supervision during the year 2015-2016.

**Dr. R. Vasudevan
Professor and Head**

Department of Aerospace Engineering

**Mr. Umar Rizwan
(Project Guide)**

Assistant Professor

**SRM UNIVERSITY
KATTANKULATHUR- 603203
CHENNAI, INDIA.**

ABSTRACT

Single Rotor Vertical Take-off and Landing system is selected due to complexity and enthralling factor. Aim of the project is to design an Unmanned Aerial Vehicle which can take off and land vertically with using single propeller in order to provide thrust. Challenge involved in the system is single rotating propeller which is main contributing element to provide lift is making the whole system unstable due to torque of power system. In case of conventional helicopter tail rotor is provided to balance the torque provided by main rotor power system again multi rotors have even number of rotating propellers which rotates in such fashion cancels the net moment about body. Though there are challenges due to unconventional design, there are certain advantages such as Symmetry of Body in all axis, shape of UAV is spherical thus it can roll through obstacles, delegate parts are enclosed in frame ensuring safety of the system. The main feature of this project is an indigenous design of a flight computer and Ground station.

KEYWORDS: UAV, flight computer, Ground station, single rotor, VTOL

CONTENTS

TITLE PAGE

ACKNOWLEDGEMENTS	i
-------------------------------	----------

CERTIFICATE	ii
--------------------------	-----------

ABSTRACT	iii
-----------------------	------------

LIST OF TABLES	vii
-----------------------------	------------

LIST OF FIGURE	viii
-----------------------------	-------------

NOMENCLATURE	xi
---------------------------	-----------

CHAPTER 1 INTRODUCTION	1
-------------------------------------	----------

1.1 History of UAV.....	1
-------------------------	---

1.2 Requirement Analysis	2
--------------------------------	---

CHAPTER 2 LITERATURE SURVEY	7
--	----------

CHAPTER 3 PRELIMINARY DESIGN	10
---	-----------

3.1 Power plant	11
-----------------------	----

3.2 Propeller Theory	12
----------------------------	----

3.3 Power	13
-----------------	----

3.4 Hovering	16
--------------------	----

3.5 Endurance	18
---------------------	----

CHAPTER 4 MODELLING	19
----------------------------------	-----------

4.1 Introduction to Catia	19
---------------------------------	----

4.1 Drafting of design	20
------------------------------	----

4.1 Material Selection	26
------------------------------	----

4.3.1Abs m30 - core body	26
--------------------------------	----

4.3.2 Aluminium sheet – spars	27
-------------------------------------	----

4.3.3 Balsa - control surfaces	29
--------------------------------------	----

4.4 Component Selection	30
-------------------------------	----

4.4.1 Motor	30
-------------------	----

4.4.2 Electronic speed controller	31
4.4.3 Servos	32
4.4.4 Battery selection	33
CHAPTER 5 THE UAV AUTOPILOT SYSTEM	34
5.1 Introduction	34
5.2 Flight computer	35
5.2.1 Microcontroller	36
5.2.2 Barometric Sensor	38
5.2.3 IMU	39
5.2.4 Stability and Control Algorithm	42
5.3 Ground Station	45
5.4 Communication and Data Handling	47
5.6 Electrical Power System	49
5.6.1 3A Mini Dc to Dc Converter	50
CHAPTER 6 ANALYSIS.....	51
6.1 Introduction to ANSYS	51
CHAPTER 7 FABRICATION.....	55
7.1 Aluminium spars fabrication	55
7.2 Core body – abs-m30	56
7.3 Control surfaces – balsa	57
CHAPTER 8 TESTING AND EXPERIMENTAL SETUP	58
8.1 Sensors test	58
8.2 Motor and servo test	58
8.3 Translatory and yawing motion / stability test	58
8.4 Six component balance test	60
CHAPTER 9 TEST RESULTS AND CONCLUSION.....	63
9.1 Six Component Test	63

9.2 Ground Station Test	66
9.3 Conclusion	67
9.4 Future scope	67
FINAL PROTOTYPE	68
APPENDIX I	69
APPENDIX II	78
LIST OF FABRICATORS	87
REFERENCE	88

LIST OF TABLES

TABLE	TITLE	PAGE
1.1	Required Specifications	3
4.1	Mechanical Properties of ABS-M30.....	27
4.2	Comparative study of materials	28
4.3	Comparative study of materials	29
4.4	Servo Specifications	30
4.5	Battery Specification	33
5.1	Teensy Specifications	37
5.2	BMP180 Specifications	38
9.1	SIX Component Test Results	62
9.2	Required Specifications	63
9.3	Required Specifications	63
9.4	Required Specifications	64

LIST OF FIGURES

FIGURE	TITLE	PAGE
1.1	The design wheel (Raymer 1991)	4
1.2	Aircraft design process (Raymer 1991)	5
1.3	Aircraft Conceptual design Process (Raymer 1991).....	6
3.1	Concept sketch Free body Diagram	10
3.2	Force in equilibrium condition.....	11
3.3	Propeller flow	12
3.4	NACA008, NACA0010 airfoils.....	16
3.5	NACA 0008 polar	16
4.1	CATIA model	19
4.2	Spar	20
4.3	Motor mount	20
4.4	Core body	21
4.5	Flaps	21
4.6	Rudder.....	22
4.7	Motor shell	22
4.8	Battery	23
4.9	Motor.....	23
4.10	Servo	24
4.11	Motor holder	24
4.12	Propeller.....	25
4.13	nut and bolt	25
4.14	Electronics	30

4.15	Avionic 3548 900- brushless motor	31
4.16	40A ESC	31
4.17	9g Servo	32
5.1	UAS System	34
5.2	In-house designed Flight computer	35
5.3	Teensy 3.2 Pin out diagram	36
5.4	BNO 055 9-Axis IMU	40
5.5	9-Axis IMU Architecture	41
5.6	9-Axis IMU Fusion.	41
5.7	Yaw Stability algorithm	42
5.8	Yaw Stability algorithm	43
5.9	Pitch, Roll Stability algorithm	43
5.10	Feedback Control loop	43
5.11	Flight Computer Block Diagram	44
5.12	Ground Station and Flight Computer Integration Block Diagram	44
5.13	Ground Station GUI	44
5.14	Avionics Instrument Panel	45
5.15	XBEE Pro Series 2.....	46
5.16	Electrical Power System	48
5.17	DC to DC Converter	48
6.1	3D Streamline Flow over rudder	49
6.2	Velocity vectors over rudder	50
6.3	3D Flow visualization over body	51
6.4	3D Flow visualization over body	52
6.5	Visualization of Stress magnitude	53
7.1	Aluminium sheet	54
7.2	3D Printed core body	55

7.3	On-Going cleaning process at SRM RPT Lab	56
7.4	In-house fabricated control surfaces	56
8.1	Entire setup for the test	58
8.2	Six component balance setup	59
8.3	Entire setup for 6 component balance test	60
9.1	SIX Component Balance Force and Moment Graph	66
9.2	Yawing Stability with Disturbances	66

NOMENCLATURE

UAV	Unmanned aerial vehicle
VTOL	Vertical take-off and landing
α	Angle of attack
β	Side slip angle
Φ	Roll angle
Ψ	Heading angle
F^b	Body coordinate frame
F^i	Inertial coordinate frame
F^s	Stability coordinate frame
F^v	Vehicle coordinate frame
F^w	Wind coordinate frame
F^{v1}	Vehicle-1 frame
F^{v2}	Vehicle-2 frame
$\mathbf{i}^b, \mathbf{j}^b, \mathbf{k}^b$	Unit vectors defining the body frame
$\mathbf{i}^i, \mathbf{j}^i, \mathbf{k}^i$	Unit vectors defining the inertial frame
$\mathbf{i}^v, \mathbf{j}^v, \mathbf{k}^v$	Unit vectors defining the vehicle frame
p_n	Inertial north position of the MAV along \mathbf{i}^i in F^i
p_e	Inertial east position of the MAV along \mathbf{j}^i in F^i
p_d	Inertial down position of the MAV along \mathbf{k}^i in F^i
\mathbf{U}	Body frame velocity measured along \mathbf{i}^b in F^b
\mathbf{V}	Body frame velocity measured along \mathbf{j}^b in F^b

φ	Roll angle defined with respect to F^{v^2}
P	Roll rate measured along \mathbf{i}^b in F^b
Q	Pitch rate measured along \mathbf{j}^b in F^b
R	Yaw rate measured along \mathbf{k}^b in F^b
θ	Pitch angle
M	Mass of the airframe
V_a	Airspeed vector
V_g	Ground speed vector
V_w	Wind speed vector
$\omega_{\frac{b}{i}}$	Angular velocity of the body frame with respect to the inertial frame

CHAPTER 1

INTRODUCTION

Unmanned aircraft Vehicle system (UAV) is associate degree rising technology with an amazing potential to revolutionize warfare and to change new civilian applications. Its integral a part of future urban civil and military applications. This technologically matures enough to be incorporated into the general public. The significance of UAV in scientific applications has been totally showed in recent years no matter missions are chosen for the UAV, their range and use can considerably increase within the future. UAV nowadays play crucial role in several public missions like border police patrolling, life surveys, training, climate observation, and native enforcement.

UAV systems describes entire system that includes aircraft, control stations and data links.

- i. Ground control station
- ii. A mission planning module
- iii. A launch and recovery system
- iv. Ground data and communication handling module
- v. Remote video terminals
- vi. Modular mission payload modules
- vii. Miscellaneous launch, recovery, and ground support equipment

1.1.HISTORY OF UAV

The FAA has adopted the acronym UAS (Unmanned Aircraft System) to reflect the fact that these complex systems include ground stations and other elements besides the actual air vehicles i.e. Unmanned Aircraft. "UAS" describes" entire system that includes aircraft, control stations and data link". The first UAV was manufactured by the Americans Lawrence and Sperry in 1916. This is known as the beginning of — attitude control, which came to be used for the automatic steering of an aircraft. They called their device the —aviation torpedo and Lawrence and Sperry actually flew it a

distance that exceeded 30 miles. The development of UAVs began in earnest at the end of the 1950s, taking advantage of the Vietnam War or the cold war, with full-scale research and development continuing into the 1970s. UAV called Fire bee. After the Vietnam War, the U.S. and Israel began to develop smaller and cheaper UAVs. These were small aircraft that adopted small engines such as those used in motorcycles or snow mobiles. They carried video cameras and transmitted images to the operator's location. It seems that the prototype of the present UAV can be found in this period. The U.S. put UAVs into practical use in the Gulf War in 1991, and UAVs for military applications developed quickly after this.

Classification of Unmanned Aircraft

- i. Fixed-wing UA: which refer to unmanned airplanes (with wings) that require a runway to take-off and land, or catapult launching these generally have long endurance and can fly at high cruising speeds.
- ii. Rotary-wing UA: also called rotorcraft UAVs or vertical takeoff and landing (VTOL) UAVs, which have the advantages of hovering capability and high maneuverability. These capabilities are useful for many robotic missions, especially in civilian applications. A rotorcraft UAV may have different configurations, with main and tail rotors (conventional helicopter), coaxial rotors, tandem rotors; multi-rotors, etc.
- iii. Blimps: such as balloons and airships, which are lighter than air and have long endurance, fly at low speeds, and generally are large sized.
- iv. Flapping-wing UA: which have flexible and/or morphing small wings inspired by birds and flying insects. There are also some other hybrid configurations or convertible configurations, which can take-off vertically and tilt their rotors or body and fly like airplanes, such as the Bell Eagle Eye UAV. Another criterion used at present to differentiate between aircraft is size and endurance.

1.2.REQUIREMENT ANALYSIS

Consider a chemical factory having malfunction in its boiler which is used to store some kind of hazardous gas. Now in such environments it is impractical to send human for

prior inspection. In such cases there is need of an autonomous system operated from safe location, such robotic system should be very rugged to sustain in devastated environment. UAV is inherently unstable thus first priority is given to hover the aircraft at particular altitude and should be able to stay in stable position for its entire course even when subjected to small disturbances. UAV should ascent at 2g acceleration provided at its maximum power. Purpose of complete system is to monitor condition of dilapidated room and surveillance. Main payload for this system considered is a light weight camera, but it can be replaced with 3 dimension LIDAR sensor to get more details of environment under supervision, some light weight sensors can also be mounted to get the chemical property of room ranging from moisture, temperature to pH and detection of harmful gases. This system is to be designed to work preferably in indoor environment. Propeller or any other moving component should be encapsulated in strong frame. As proposed system is very unique in design and to achieve desired stability and performance characteristics is not easy task due to unconventional skeleton, though system can be made analogues to conventional vertical Take-off and Landing Vehicles such as multi rotors and Helicopter. Following are required design specifications to be achieved in order to satisfy the project needs.

Table 1.1 Required Specifications

Sr. No	Description	Value (approximate)	Unit
1	Maximum All Up Weight	1	Kg
2	Payload Weight	0.2	Kg
3	Maximum Climb Rate	3	m/s
4	Vertical Acceleration	2g	G
5	Maximum Level velocity	5	m/s
6	Endurance	10	Min
7	Range	200	M
8	Service ceiling	200	M

To achieve desired performance characteristics we start with design process of UAV system taking conventional UAV as reference. The design of any concept is the using of geometry and mathematics to break down a part into its components in order to describe something that is going to be built (Raymer, 1991). Design of UAV system can be categorized in tree major domains: the conceptual design, preliminary design and the detailed design. The conceptual design mainly deals with configuration, size, weight and performance based on the mission specification and requirements (Roskam, 1985). The preliminary design then advances these concepts by individually designing and sizing all of the major components of an aircraft. The final part of the process is the detailed design in which all of the major components are broken up and the internal structures developed and the manufacturing considerations made (Raymer, 1991). At the end of the conceptual design it should be promising to establish the UAV's stability and performance characteristics which should meet, if not exceed the mission requirements.

The beginning of aircraft design is unclear as like so many design processes many of the design factors will be changed during the course of the design, therefore creating an iterative design loop (Raymer, 1991) such as one shown in Figure 1

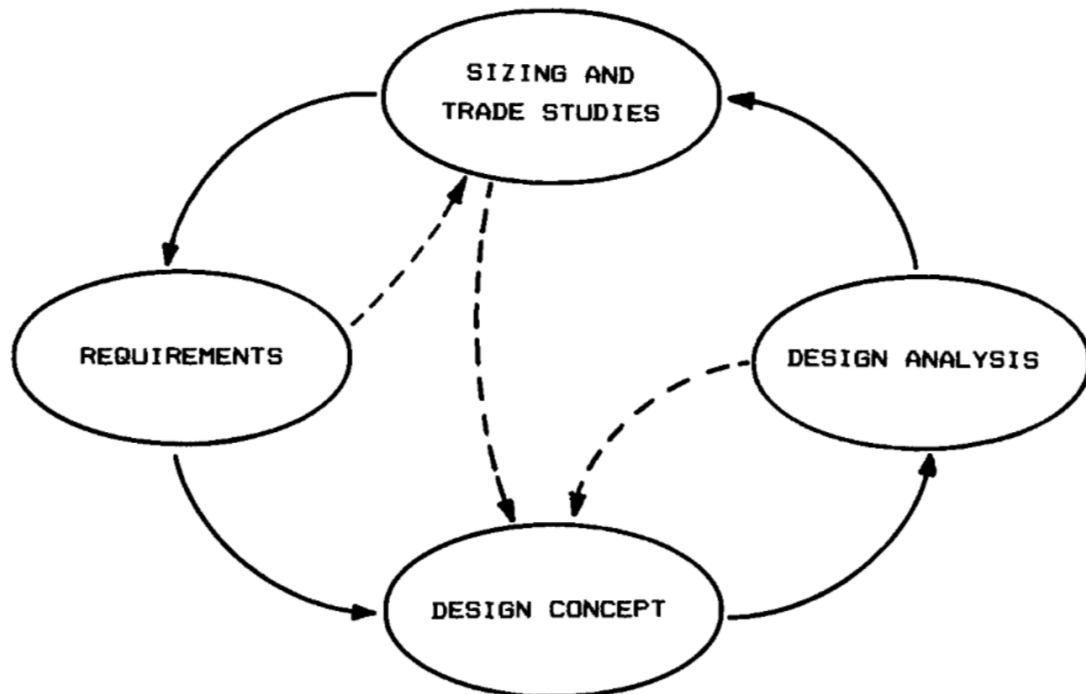


Figure 1.1: The design wheel (Raymer, 1991).

The design process for a UAV begins with the development of mission specifications and profiles followed by the determination of the payload to match the mission specification (Roskam, 1985). Once the payload has been determined it is then possible to estimate the total weight of the UAV. This can then be compared to research about previous UAV's and checking the calculations against the trend. Once the weight estimation has been verified the next step is to generate the constraint graphs. The constraint graphs determine the feasible design region at which the required mission specifications can be met (Roskam, 1985). Once the feasible design region has been found a point is then picked to give the optimum power loading and wing loading. This point provides both the wing area and the maximum power required for flight including climb. The next stage of the conceptual design is to decide on a configuration for the UAV. This entails the type of control surface and the placement of the power plant. During this process several designs should be generated and their benefits evaluated before finally concluding on a design.

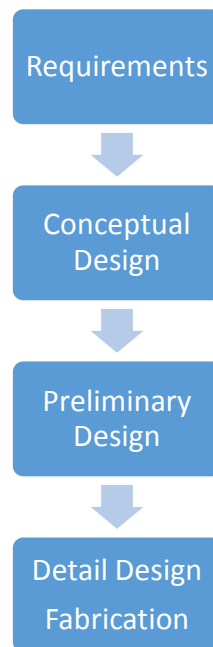


Figure 1.2: Aircraft design process (Raymer 1991)

After this it is possible for the design to move into the preliminary stage. The main lifting element can be designed and once all of the systems components are finalized

the fuselage can be designed also. After this it is then possible to make preliminary weight estimates and again verify that the UAV is within its design constraints.

Once the configuration is finalized and all the major components sized it is then possible to develop the detailed design of the UAV. This involves the design of the internal structure. The structure can be designed in one of two ways. The first is to design the structures by hand. The number of ribs and the positions of the main spar/s can be determined through a series of stress calculations and design choices (Raymer, 1991). The second option is to use topology optimization to determine the stiffest structure possible whilst reducing the weight. During the design of the internal structure it is also important to take into account the manufacturing restrictions as these can cause large components of the design to be reconsidered if not accounted for. A combination of CFD and stability analysis can then be used to determine the aerodynamic and flight characteristics of the aircraft. Once each of these processes is complete it is then possible to build a detailed final model of the design and find the performance characteristics of the aircraft.

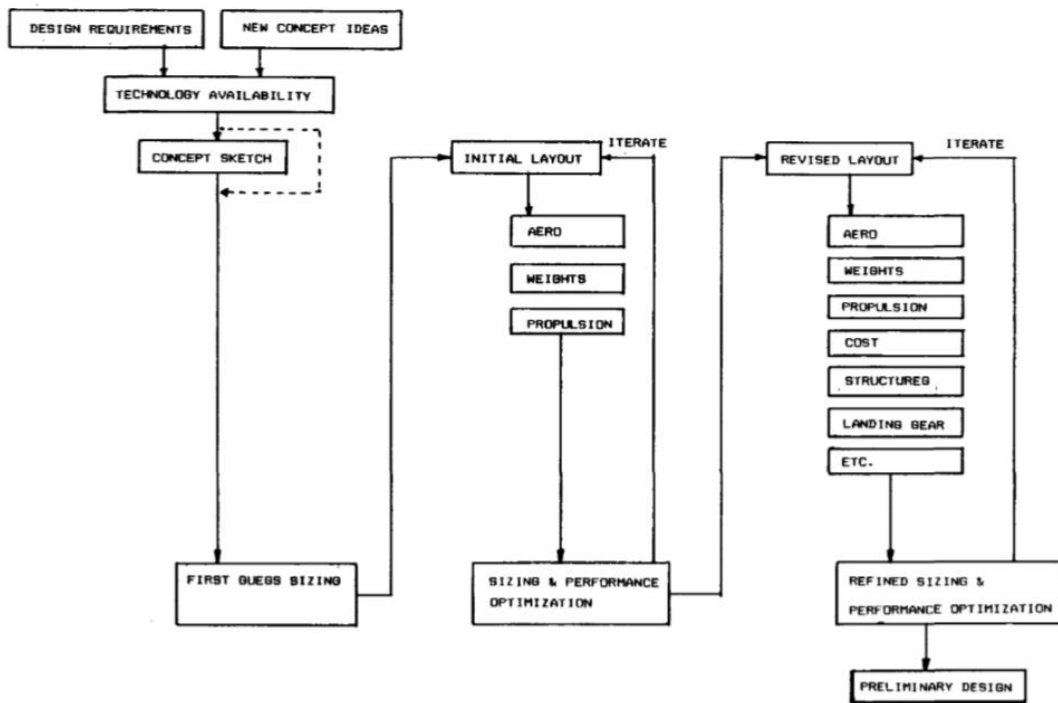


Figure 1.3: Aircraft Conceptual design Process (Raymer 1991)

CHAPTER 2

LITERATURE SURVEY

The power plant systems that were studied in Rapid Sizing Methodologies for VTOL UAVs, Jonathan D. Keith are (i) Combined Power plant Systems, in this type of system, weight is reduced by making optimum use of a single propulsion system which is used for hovering as well as forward flight. In order to demonstrate relative accuracy of generated equation from the data, the generated equation is used with the empty weight values from each aircraft in ANSER wheel to calculate each aircraft's takeoff gross weight. This equation-generated value for takeoff gross weight is then compared against the actual take-off gross weight value to determine that percent error caused by using the generated equation. (ii)Augmented Propulsion System for Hover, is used for aircrafts where the generated propulsion is augmented during the hover flight stage where Data from the weight data of VTOL aircraft is used to evaluate the trend line of the parameters and is compared with the remaining aircraft with a 15.7% standard deviation.(iii)Combined Power plants for Hover, system uses a single propulsion system for both hovering as well as forward flight along with additional power plant for thrust augmentation during hover flight stage. Using the same approach taken with the first two categories, a trend line is generated and the original data are tested against this trend line, yielding error results with a standard deviation of 13.7%.

The engines that are studied in ANDRÁS FÜLEKY, Driving systems of unmanned air vehicles, (2004) are: combustion engine, it is used to power a propeller which uses the ambient air for its operation. The IC engines are also used to generate power for an UAV which have low operational costs and have its advantages over combustion engines. Micro Jet engines have also become an option to power an UAV due to development of micro-engineering. The engine provides thrust by combusting the fuel in the combustion chamber which rotates the turbine blades which in turn rotates the compressor blades for further intake of air. Remaining exhaust gas provides the necessary thrust velocity. These were the Aerobe engines which relies on the atmospheric air for their operation. The Rocket engine (Anaerobe engine) which carry

their own fuel and oxidizer for combustion operation. The most widely used rocket engine is the solid propellant rocket which is compact and are easily manufactured. A rocket engine can be used to launch the UAV to a certain height before separating from it. After which the UAV can glide or operate using an electric engine. Electric motors and high capacity batteries have been in development and are used to power small aircrafts and UAVs. These are easy to operate and can be switched on/off mid-air also. The flight time of an UAV depends upon the type of battery used and the endurance efficiency is reduced due to the usage of motor brushes that operate at high rpm which produces heat and reduction in current supply efficiency.

There are different types of rotorcraft configurations available it is stated in A. Imam and R. Bicker , Design and Construction of a Small-scale Rotorcraft UAV System, January 2014 is that design phase of rotorcraft system involves five key elements (i) virtual design environment selection (ii) hardware components selection (iii) avionic system design and integration (iv) vehicle design and construction (v) performance and reliability evaluation. paper further classifies the rotorcrafts as Conventional main rotor (CMR) configuration which is basically helicopter with large lifting head rotor rotating normal to horizontal plane and a small rotor rotating normal to vertical plane to provide counter torque to vehicle body, next it discuss about Coaxial rotors (CAR) configuration in which two counter rotating propellers cancel torque and provide lift element to body differential angular velocities provides yawing moment to rotorcraft. Tandem rotors (TR) configuration consist of two large rotors maintained at specific offset distance. It is capable of carrying heavy payloads Multi-rotors (MR) configuration uses more than two fixed pitch propellers. Maneuver is achieved by differential angular velocities.

Most of VTOL UAV has more multi rotor configuration, Japans defense ministry's Technical Research Team invented single rotor VTOL UAV in 2011 in a press conference, other single rotor UAV are built by hobby enthusiast which having large symmetrical wings in X and Y axis and propeller rotating along Z axis, which provides enough inertial component to resist the torque produced by motor. Design of Single rotor VTOL UAV is challenging task because lack of previous data. Available options

are made by hobby enthusiast which are designed based on hit and trial method and no proper design and modeling approach is used.

Mathematical modelling study is mostly related to helicopter, which is very similar our design but having extremely different Lift vector. NASA Technical Memorandum 84281 A Mathematical Model of a Single Main Rotor Helicopter for Piloted Simulation, Peter D. Talbot, Bruce E. Tinling, William A. Decker, and Robert T. N. Chen, September 1982, explains about flying qualities of single main rotor helicopter, in which forces and moments are calculated in hub-wind axis system and expressed in body system, A linearized 6DOF model is developed which represents dynamics of helicopter on small disturbance.

MS thesis by Jon Bernhard Høstmark,"Modelling Simulation and Control of Fixed-wing UAV: CyberSwan", developed mathematical model in MATLAB/Simulink using AeroSim toolbox and AeroSonde CyberSwan template model is used for aerodynamic coefficients, mass and inertia terms. PID is tuned for the perturbation with respect to equilibrium point.

CHAPTER 3

PRELIMINARY DESIGN

Mainstream idea to design a new VTOL UAV is to make a single rotor spherical system. Having only one propeller to lift the spherical body in air challenge faced is torque produced by power plant tend to rotate whole vehicle in opposite direction of rotation of propeller. Solution to this is provided using control surfaces to vector the thrust component in desired magnitude which will produce equal and opposite torque applied by power plant in favourable direction to stabilize the system.

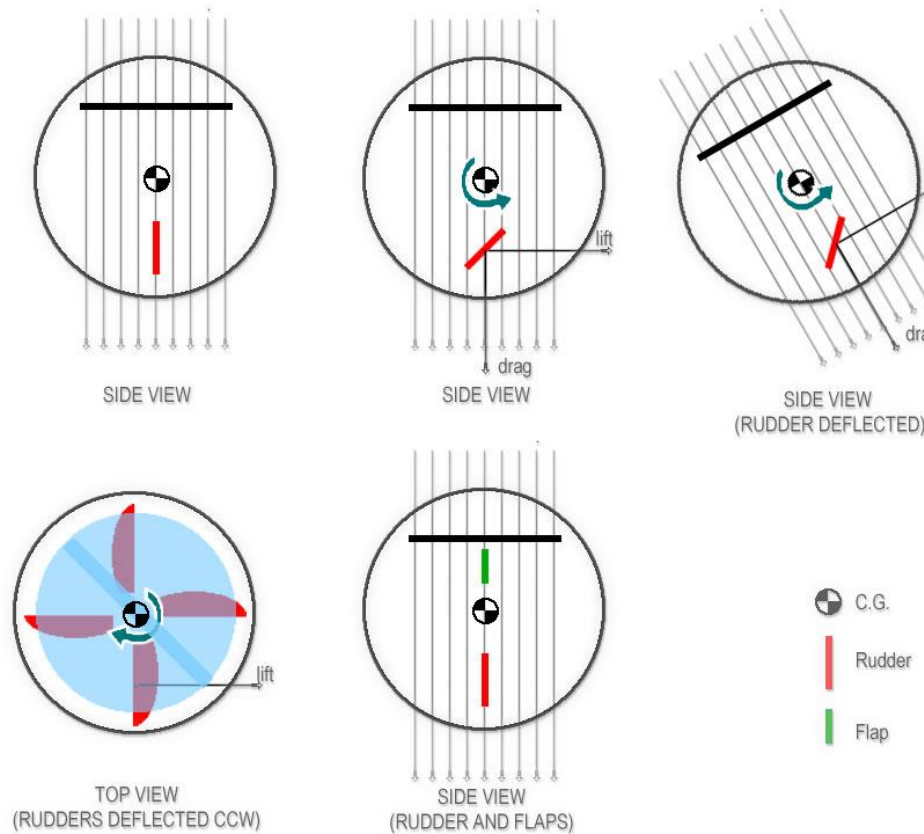


Fig 3.1 Concept sketch Free body Diagram

As mentioned in figure conceptual design and effect of propeller rotation is challenged by deflecting control surfaces to change the direction of thrust and to achieve stability

3.1. POWER PLANT

As mentioned in requirements specification all up mass of UAV is considered to be 1kg at max which yields 9.81 N force, to hover at particular altitude power plant should provide equal thrust in upward direction.

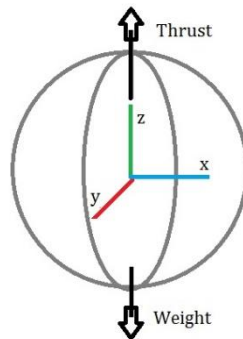


Fig 3.2 Force in equilibrium condition

Figure 1.4 shows thrust provided by power plant in Z axis upward and weight acting downwards, equating both for hovering flight thrust required will be equals to weight of aircraft

$$T = m \times g \quad (1)$$

$$m = 1 \text{ kg}$$

$$g = 9.81 \frac{\text{m}}{\text{s}^2}$$

$$T = 9.81 \text{ N}$$

9.81 Newton is required thrust to hover at an altitude closer to sea level.

For climbing to a particular altitude 2g acceleration is considered at maximum power.

$$T_{max} = 9.81 \times 2 = 19.61 \text{ N} \quad (2)$$

$T_{max} = 19.61 \text{ N}$ is maximum required thrust, hence power plant is to be selected which gives approximately 20 N thrust. Considering size of UAV Electric motor is most preferred source of power. Electric Brushless DC motors proved most efficient power plants of its class and easily available in market with suitable propeller combination.

following are Brushless DC motors available in market, All data is taken assuming 3 Cell 11.1 Volt LiPo battery, propeller size is given as diameter x pitch in inches.

3.2. PROPELLER THEORY

The Thrust of a propeller depends on the volume of air accelerated per time unit, on the amount of the acceleration, and on the density of the medium. Based on momentum considerations, it can be expressed by the following formula:

$$T = \frac{\pi}{4} D \left(v + \frac{\Delta v}{2} \right) \rho \Delta v \quad (3)$$

T – thrust

D – propeller diameter

v – velocity of incoming flow

Δv – additional velocity acceleration by propeller

ρ – density of air

Side view of the stream tube passing through a propeller

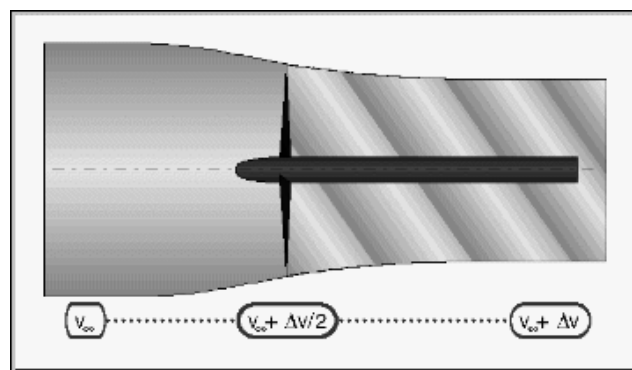


Fig 3.3 Propeller flow

3.3. POWER

$$P_a = T \times v \quad (4)$$

Efficiency of a propeller is defined as the ratio of available power to the engine power which is

$$\eta = \frac{P_a}{P_{motor}} = \frac{T \times v}{P_{motor}} \quad (5)$$

Power absorbed by propeller

$$P_{motor} = T \left(v + \frac{\Delta v}{2} \right) \quad (6)$$

Relation between Velocity-power-diameter

$$v = \eta \left(\frac{2P}{2\pi\rho D^2(1-\eta)} \right)^{\frac{1}{2}} \quad (7)$$

Maximum Power

At maximum power considering maximum potential in voltage and maximum current in Amps.

$$P_{max} = V \times I \quad (8)$$

$$P_{max} = 11.1 \times 40$$

$$P_{max} = 444 \text{ watts}$$

let us consider UAV will hover at half of maximum power.

$$P_{hover} = \frac{P_{max}}{2} \quad (9)$$

$$P_{hover} = 222 \text{ watts}$$

Maximum RPM of motor can be calculated by

$$N = kv \times V \quad (10)$$

$$N = 1100 \times 11.1$$

$$N = 12210 \text{ RPM}$$

Torque produced by power plant at maximum power

$$\begin{aligned} P_{max} &= \frac{2 \times \pi \times N \times \tau_{max}}{60} & (11) \\ \tau_{max} &= \frac{P_{max} \times 60}{2 \times \pi \times N} \\ \tau_{max} &= 0.3472 \text{ Nm} \end{aligned}$$

Now this torque will tend to rotate entire body to opposite direction of propeller rotation. To eliminate this effect and to make aircraft stable thrust produced by propeller should be vectored to give resisting moment to torque.

Thrust vectoring can be achieved by deflecting rudder as shown in figure 1.4.

Lift due to 4 rudders and distance of lift from centre of Z axis will provide moment around Z axis. Total lift required at maximum power to stabilize the UAV is.

$$\tau_{max} = 4 \times L_{rudder} \times lr \quad (12)$$

$$L_{rudder} = 0.8681 \text{ Newton}$$

lr - distance between point where lift is acting on rudder to centre of axis which we assume acts at 0.1m away from axis considering exactly below half of the propeller blade semi span.

(13)

$$L_{rudder} = \frac{1}{2} \rho \times v^2 \times S \times C_L$$

C_L is dimensionless coefficient of lift and depends upon Reynolds number, angle of attack and geometry of body

(14)

$$Re = \frac{\rho v d}{\mu}$$

Now C_L of different types of NACA thin airfoils are studied by vortex lattice method using XFOIL [4] from velocities ranging from 10m/s and 20m/s. also at different angle of attack from 0 to 20 degree or at $Re= 120,000$.

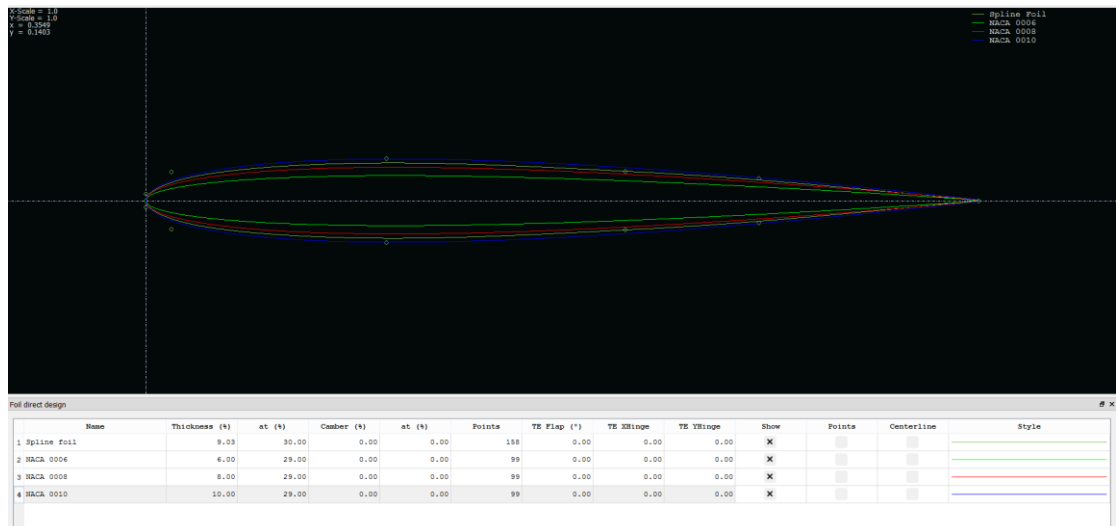


Fig 3.4 NACA008, NACA0010 airfoils

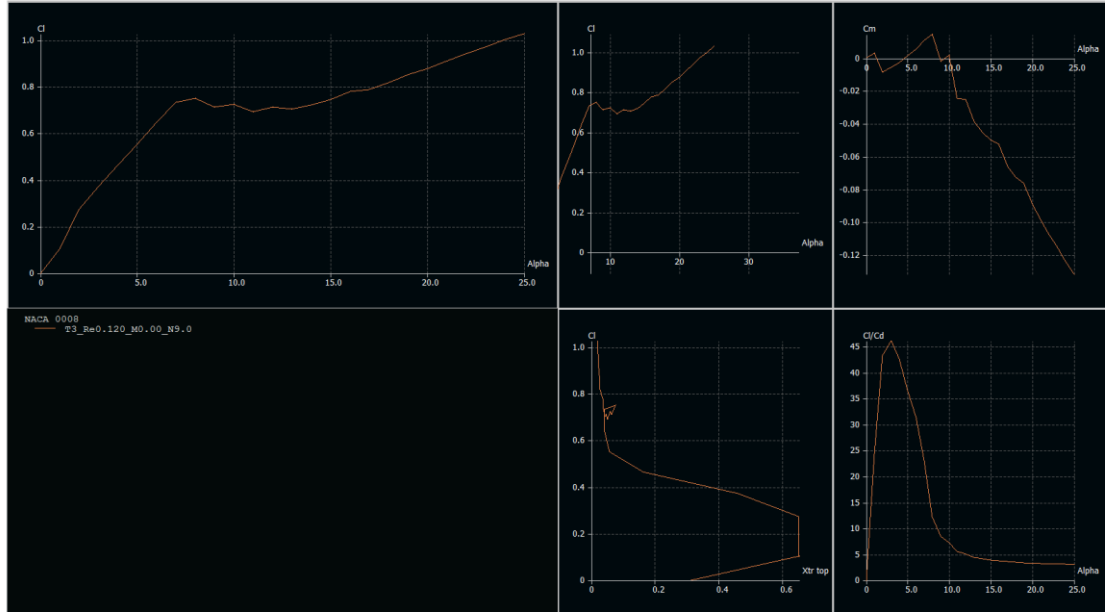


Fig 3.5 NACA 0008 polar

From above analysis C_L is taken 1 at 20° angle of attack.

$$L_{rudder} = 1.085 \text{ Newton}$$

$$0.8681 = \frac{1}{2} \times 1.225 \times 15^2 \times S \times 1$$

$$S = 0.0063 \text{ m}^2$$

Surface area of each rudder is calculated as 0.0063 m^2 .

$$L_{flap} = \frac{1}{2} \times 1.225 \times 15^2 \times 0.003 \times 1$$

$$L_{flap} = 0.4134 \text{ Newton}$$

3.4 HOVERING

Propellers:

Diameter (D) = 13.6 inch

Pitch = 6.5 inch

$$\text{Area}(A) = 0.25 \times \pi \times D^2 \\ = 145.26 \text{ inch}^2$$

$$\text{Propeller sweep area } (A_{ft}) = A \times 0.006944444 \\ = 1.0088 \text{ ft}^2$$

At half throttle:

$$P_{input(hover)} = V \times I_{hover} \quad (14)$$

$$P_{input(hover)} = 11.1 \times 20$$

$$P_{input(hover)} = 222 \text{ Watts}$$

$$P_{input(hover)} = \frac{222}{745.7} \text{ hp}$$

$$P_{input(hover)} = 0.2977 \text{ hp}$$

power loading:

$$P_L = \frac{P_{input} \times n}{A_{ft}} \quad (15)$$

$$P_L = \frac{0.2977 \times 0.85}{1.0088}$$

$$P_L = 0.25 \text{ hp}$$

Thrust Loading:

$$T_{LH} = 8.6859 \times P_{LH}^{-0.3107} \text{ lbf} \quad (16)$$

$$T_{LH} = 3.31339 \text{ lbf}$$

Endurance

At hovering:

$$t_{hover} = \frac{60 \times \frac{(C)}{1000}}{I_{hover}} \times N_{battery} \quad (17)$$

$$t_{hover} = \frac{60 \times \frac{3300}{1000}}{20} \times 1$$

$$t_{hover} = 9.9 \text{ mins}$$

At full throttle

$$t_{total} = \frac{60 \times \frac{(C)}{1000}}{I_{total}} \times N_{battery} \quad (18)$$

$$t_{total} = \frac{60 \times \frac{3300}{1000}}{40} \times 1$$

$$t_{full \throttle} = 4.95 \text{ mins}$$

3.5 ENDURANCE

In case of electric power plant battery capacity is given ampere-hour. An ampere hour (abbreviated Ah, or sometimes amp hour) is the amount of energy charge in a battery that will allow one ampere of current to flow for one hour. Thus hovering endurance can be calculated from following relation.

$$Ah = t \times I \quad (19)$$

$$3.3 = t \times 20$$

$$t = 0.165 \text{ hour}$$

$$t = 9 \text{ minutes } 9 \text{ secs}$$

thus the selected battery of 3300mAh rating gives approximately 8 minutes of hovering time.

Note that these calculations are only valid for when the incoming air is accelerated from a standstill - for example when hovering.

CHAPTER 4

MODELLING

4.1 INTRODUCTION TO CATIA

The entire designing of the spherical single rotor UAV has been done in CATIA V5 software. CATIA is a process-centric computer-aided design/computer-assisted manufacturing/computer-aided engineering system that fully uses next generation object technologies and leading edge industry standards. It enables users to simulate the entire range of industrial design processes from initial concept to product design, analysis, assembly, and maintenance. It covers mechanical and shape design, styling, product synthesis, equipment and systems engineering, NC manufacturing, analysis and simulation, and industrial plant design.

Multiple prototypes have been designed in CATIA and the following sketch shows the final revised edition of prototype in fig 4.1

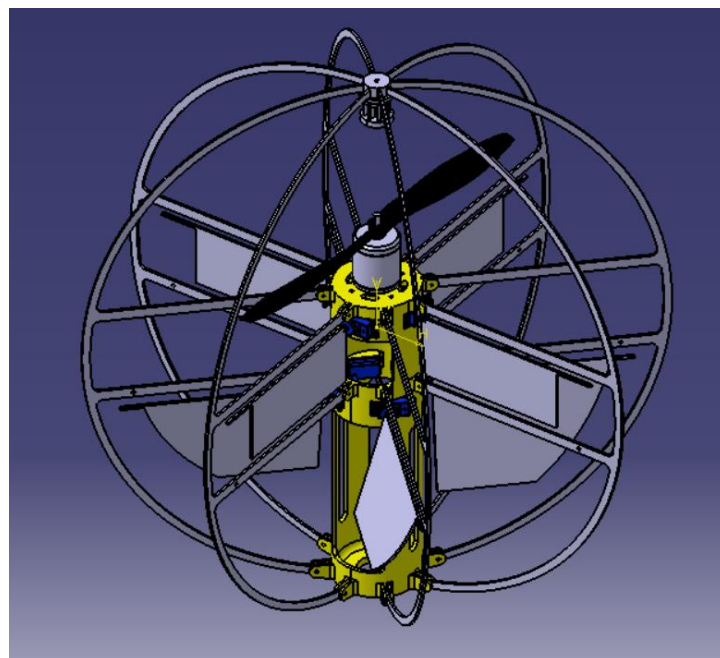


Figure 4.1 Final prototype of UAV in CATIA

4.2 DRAFTING

The drafting of every component of the spherical single rotor uav are shown in the figures given below.

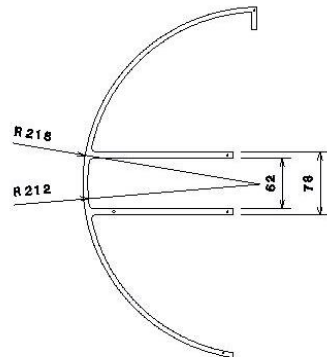


Figure 4.2 Spar

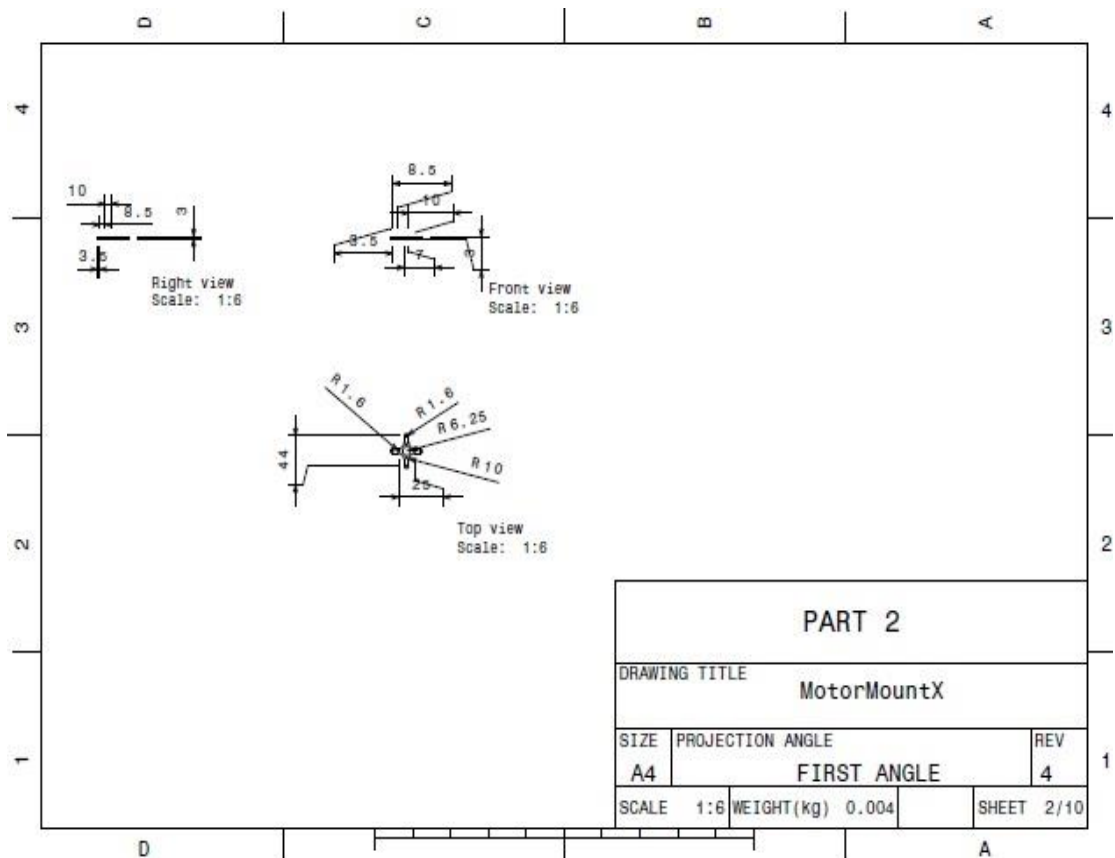


Figure 4.3 Motor mount

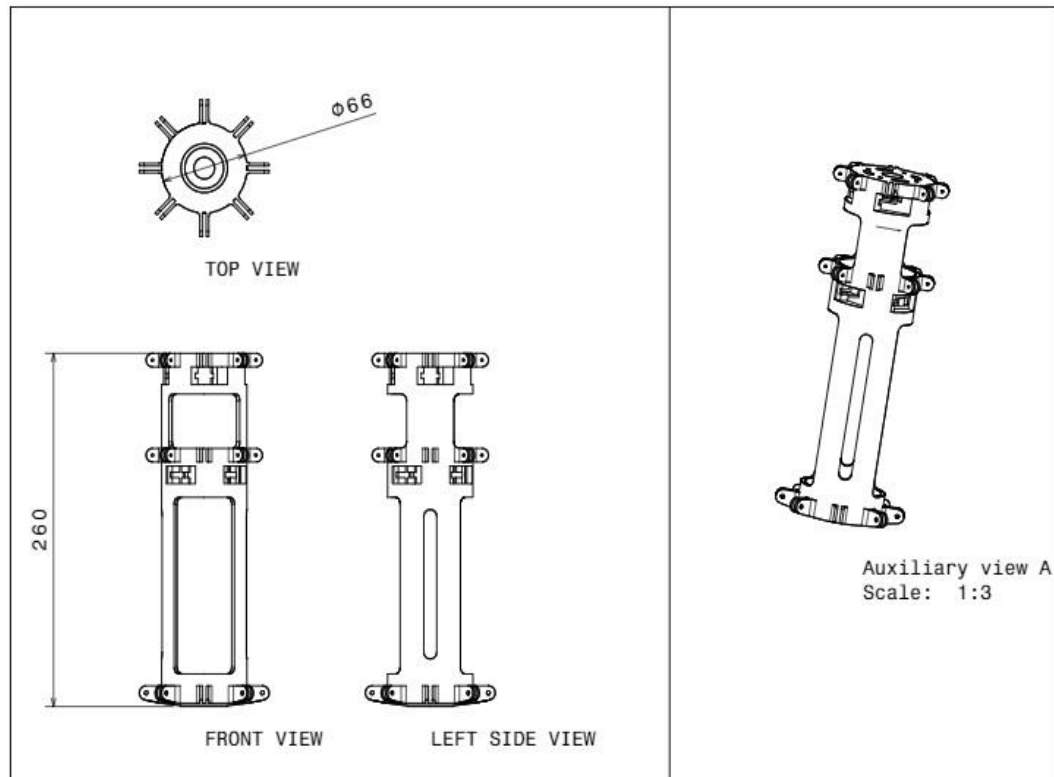


Figure 4.4 Core body

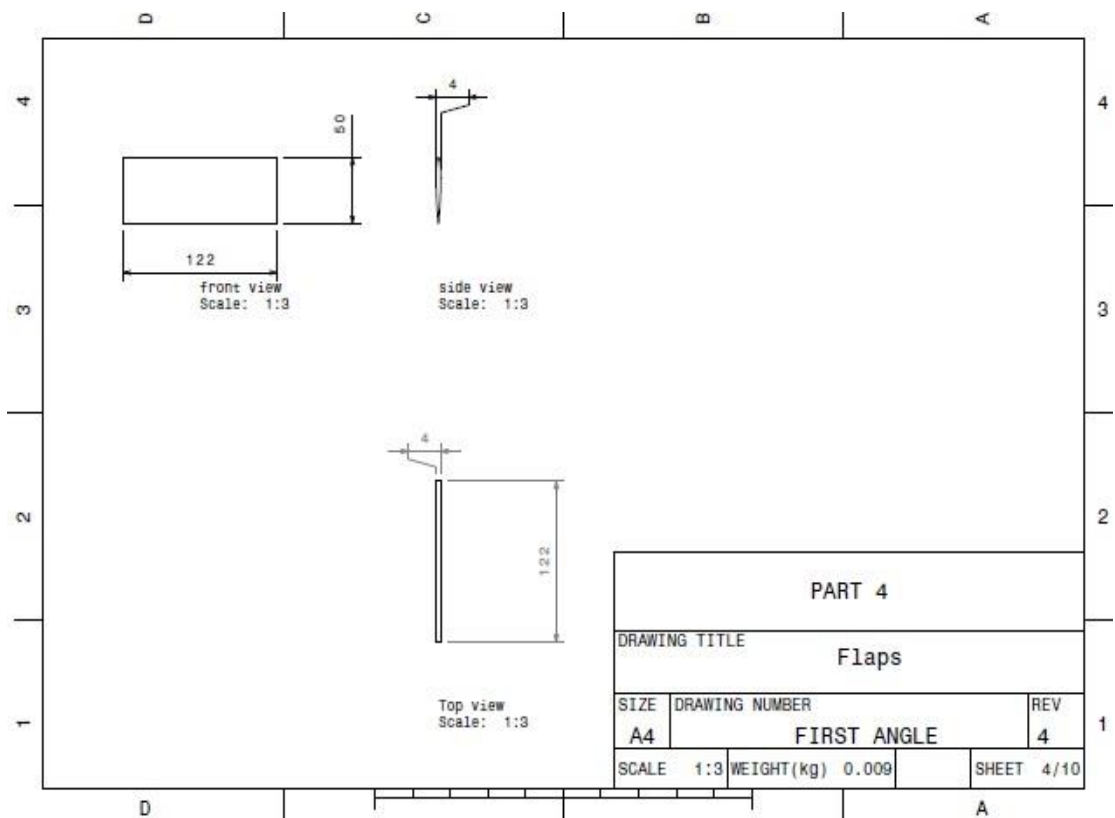


Figure 4.5 Flaps

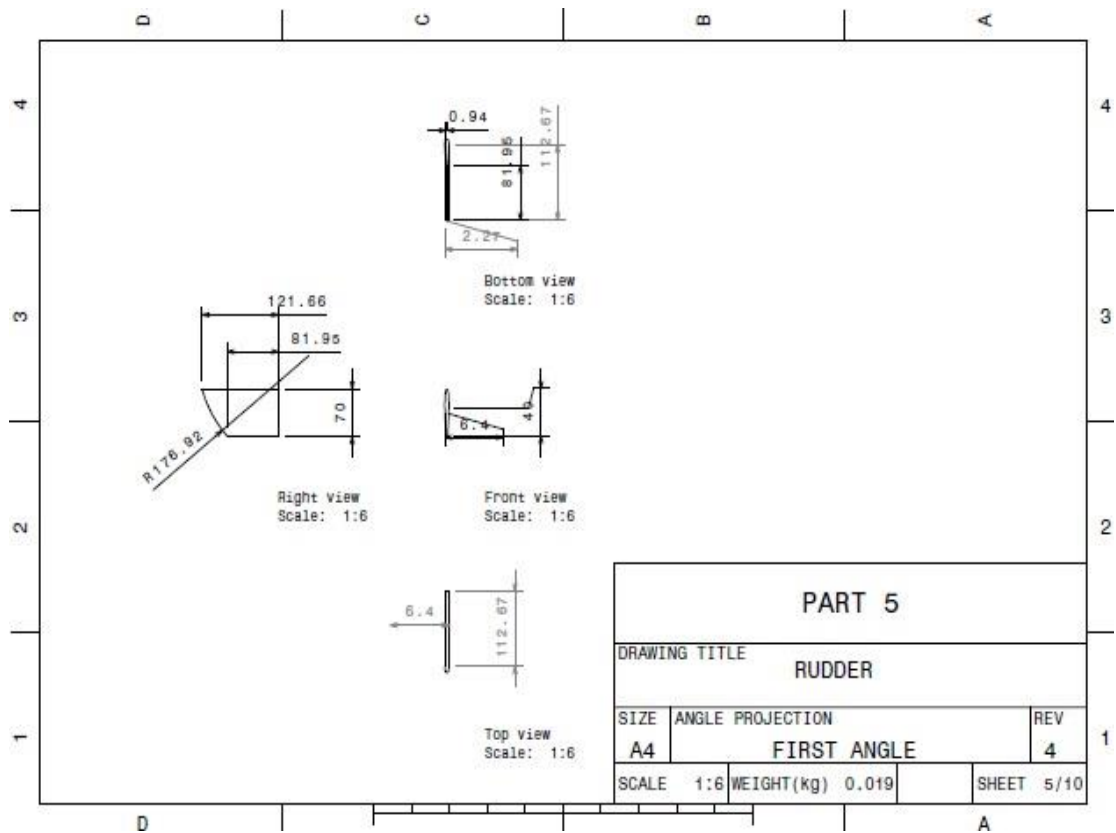


Figure 4.6 Rudder

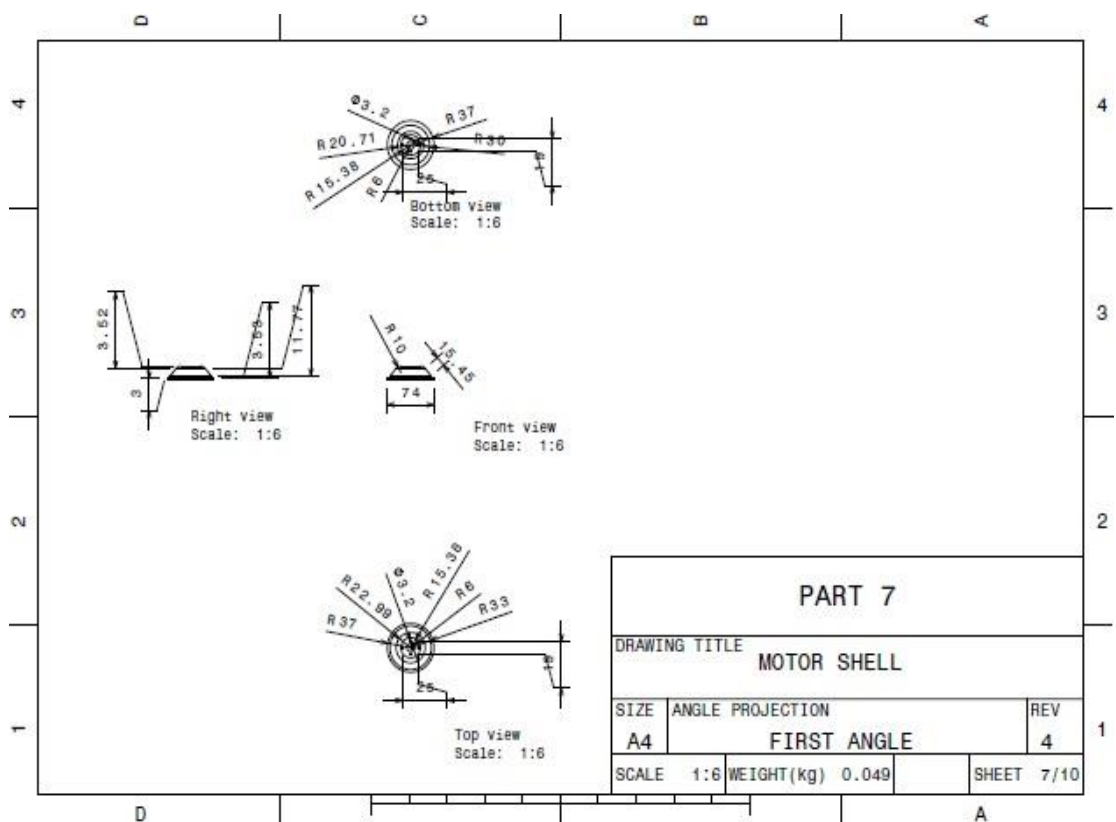


Figure 4.7 Motor shell

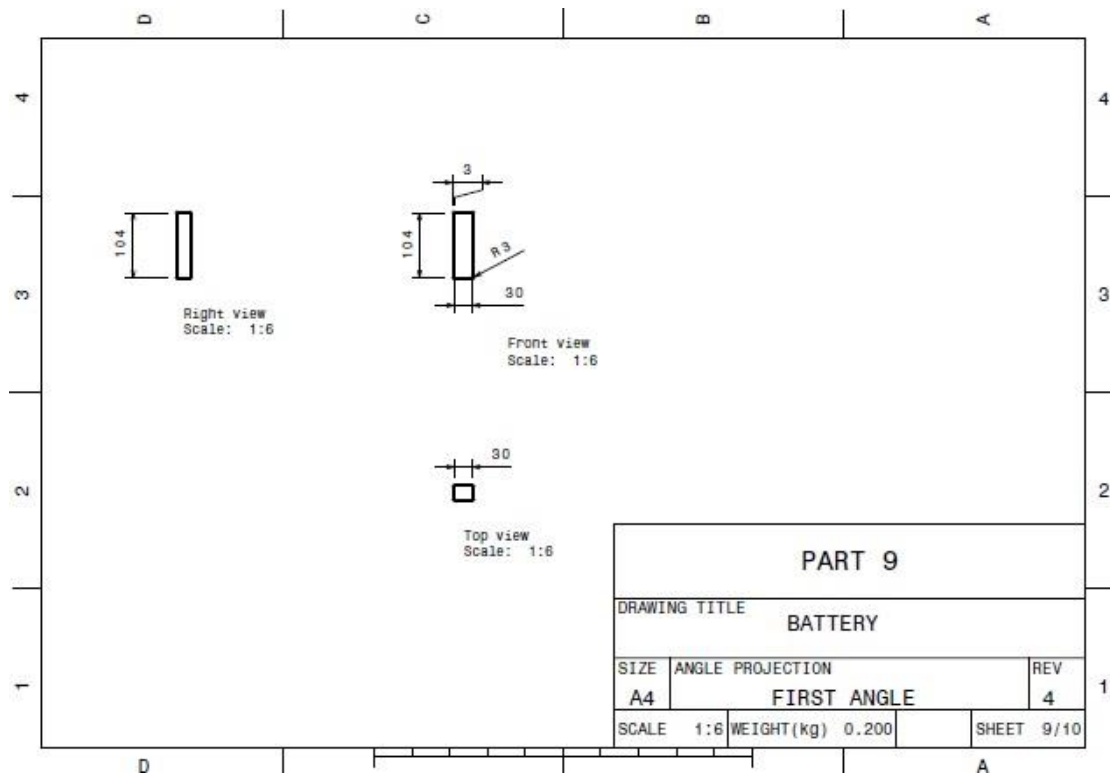


Figure 4.8 Battery

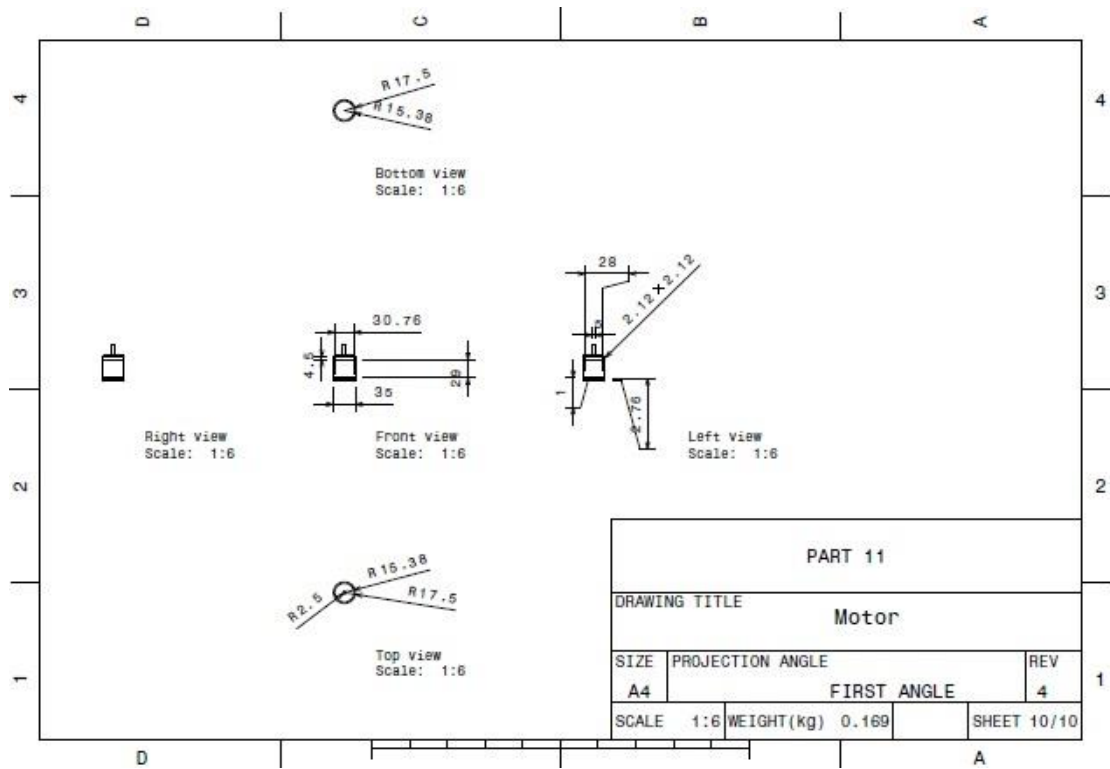


Figure 4.9 Motor

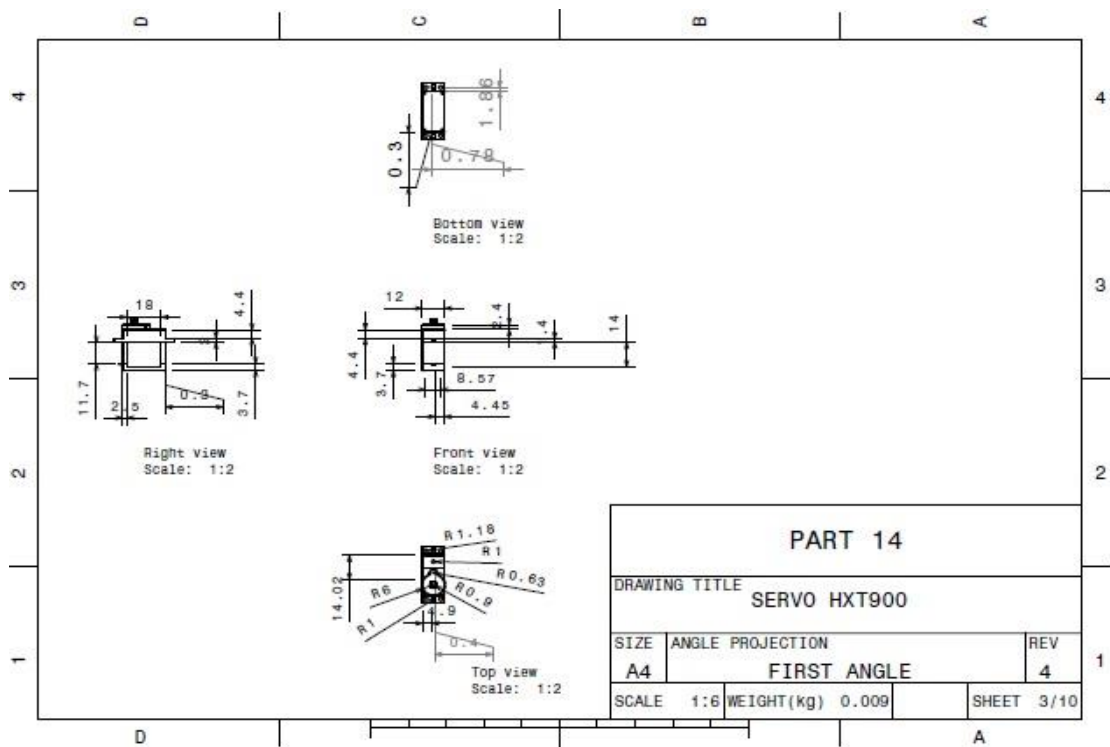


Figure 4.10 Servo

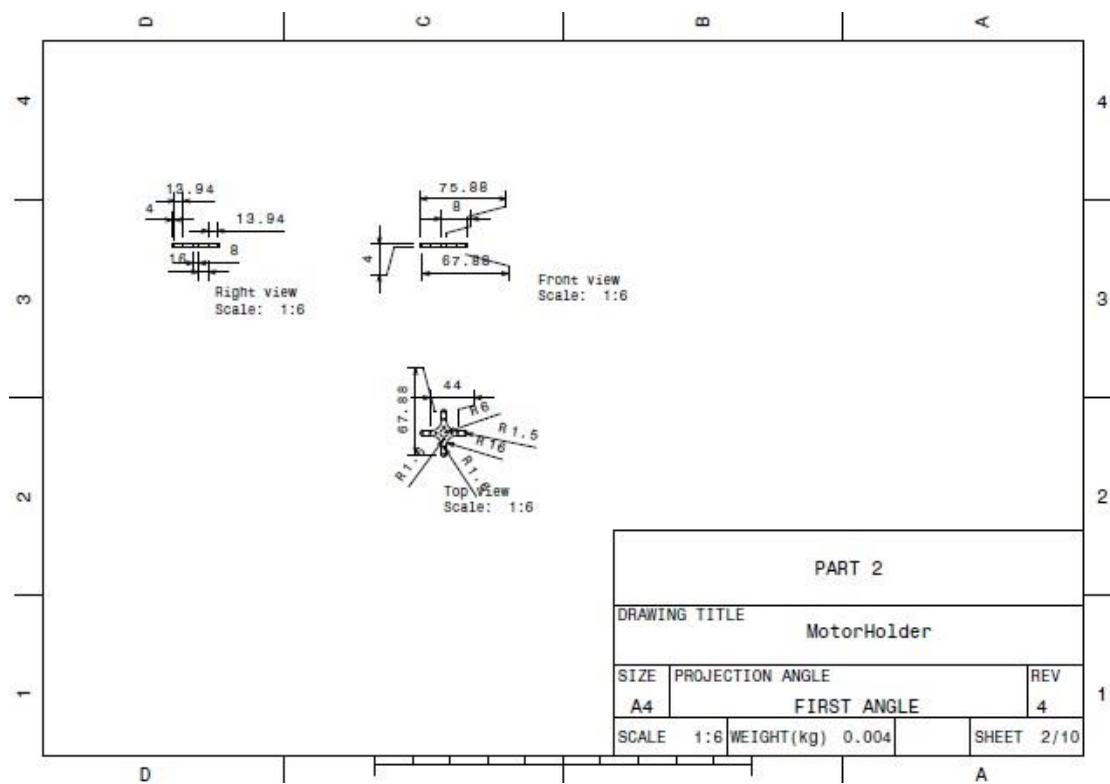


Figure 4.11 Motor holder

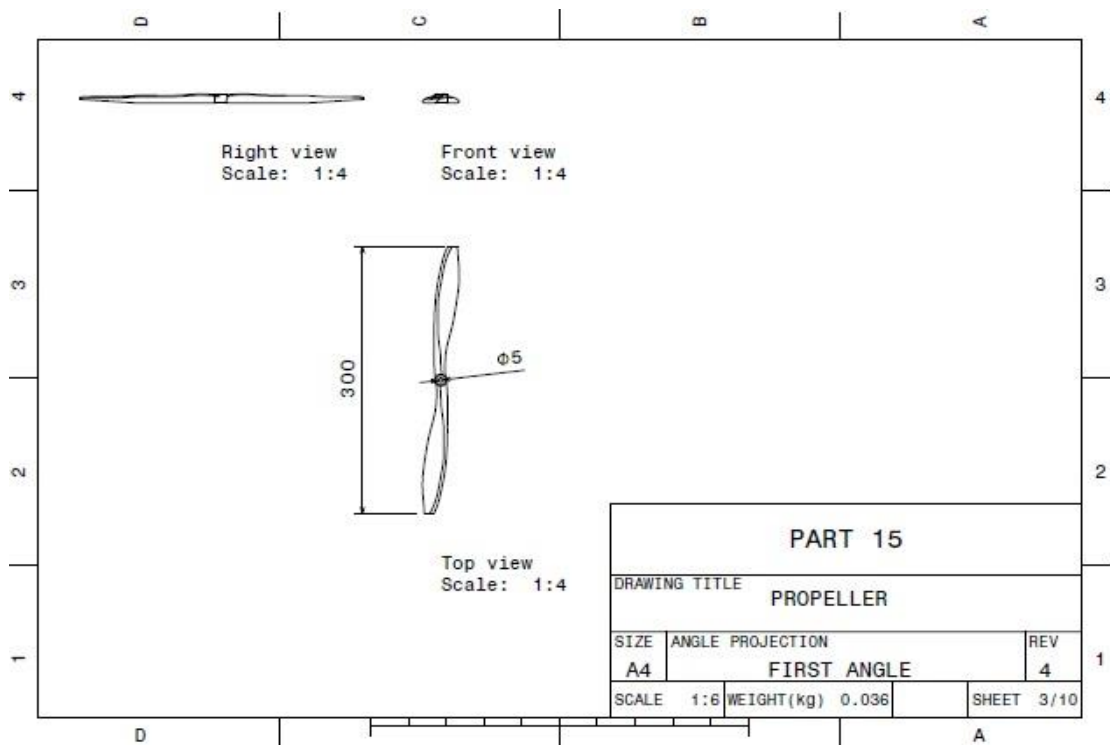


Figure 4.12 Propeller

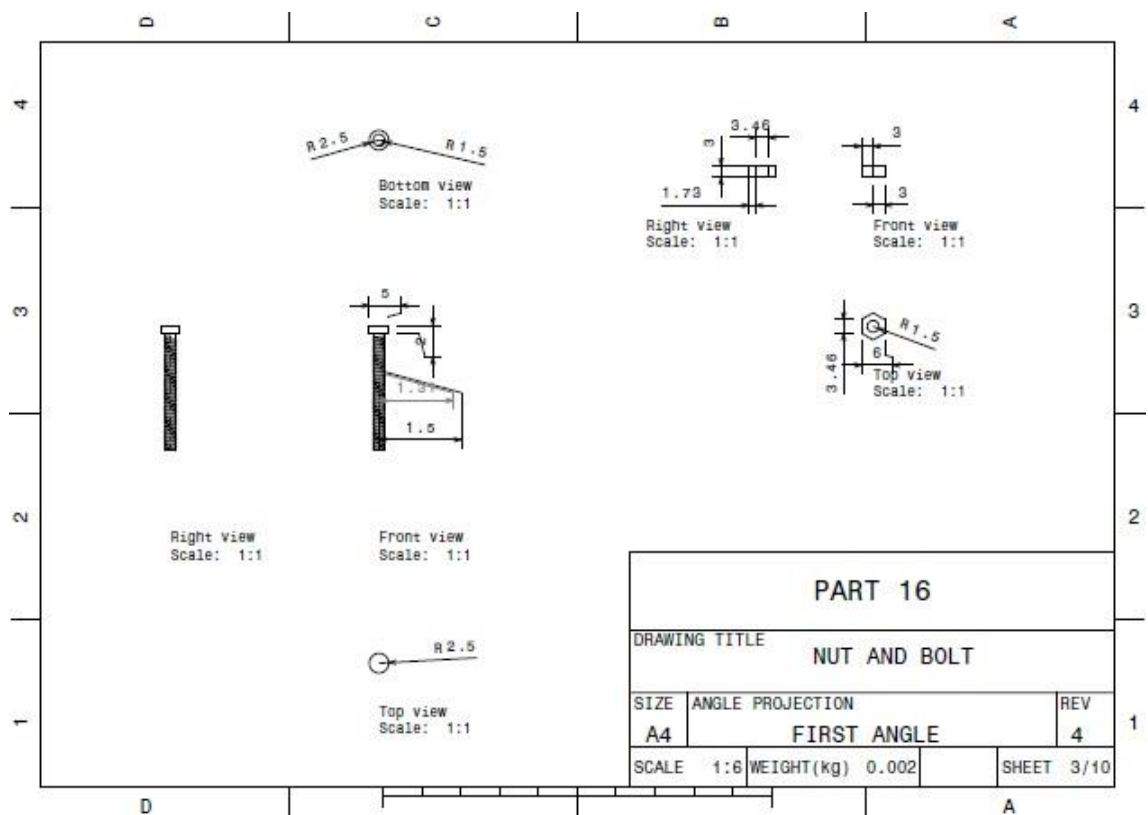


Figure 4.13 nut and bolt

4.3 MATERIAL SELECTION

Selection of an appropriate material is a vital part of almost all engineering designs. Based on the design requirements of our UAV and considering various factors which materials depend on such as: Strength, stiffness, ductility, fracture toughness, fatigue and creep which are categorized under mechanical properties. Density, melting point, thermal/electrical conductivity grouped under physical properties and other factors such as Cost, corrosion and formability. The materials selected for the various parts of our model, after a thorough study of various materials and its utilization, are as follows:

4.3.1 ABS M30 - CORE BODY

Acrylonitrile butadiene styrene (ABS) commonly known as thermoplastic polymer and has a chemical formula $(C_8H_8)_x \cdot (C_4H_6)_y \cdot (C_3H_3N)_z$. ABS-M30, grade of ABS, has been studied as it is most suitable for 3D printing and prototyping. The glass transition temperature of this material is about 108 °C. ABS-M30 is amorphous in nature and hence has no true melting point. The most important mechanical properties are impact resistance and toughness. ABS-M30 has Greater tensile, impact, flexural strength and Layer bonding than standard ABS. It is a multipurpose material as it is excellent for form, fit and functional applications.

Table: 4.1 Mechanical Properties of ABS-M30

MECHANICAL PROPERTIES	VALUE	UNIT
Tensile Strength	36	MPa
Tensile Modulus	2,400	MPa
Tensile Elongation	4	%
Flexural Strength	61	MPa
Flexural Modulus	2,300	MPa
Glass transition	108	°C
Density	1.04	g/cm ³
Heat deflection temperature	96	°C
IZOD Impact, notched	139	J/m

4.3.2 ALUMINIUM SHEET - SPARS

The material requirements of spars are high fatigue strength, toughness, high melting point and high compressive and tensile strength as it assigned to be the frame for the core body and hence needs to protect the core from harsh surroundings and any physical damage. After a comprehensive study of aluminum, acrylic and Lexan, we have zeroed on Aluminum 2024-T3 grade. It is found to have high mechanical properties along with good machinability and surface finish capability.

Table: 4.2 Comparative study of materials

MATERIAL PROPERTIES	ALMINIUM	ACRYLIC	LEXAN	UNITS
Density	2.77	1.17	1.2	g/cm ³
Elastic modulus	73	32	2.3	GPa
Elongation at Break	16	3	120	%
Fatigue Strength	140		6.9	MPa
Melting onset	502	175		°C
Shear Modulus	28	1.7	0.8	GPa
Shear Strength	285		70	MPa
Specific heat capacity	870	1260		J/kg-K
Strength to Weight Ratio	177	60	55	kN-m/kg
Tensile Strength	350	70	62	MPa
Thermal Conductivity	120	0.19	0.2	W/m-K
Thermal Expansion	22.8	75	68	μm/m-K
Fracture toughness	25			MPa-m ^{1/2}

4.3.3 BALSA - CONTROL SURFACES

Balsa wood is a natural cellular material with excellent stiffness-to-weight and strength-to-weight ratios as well as superior energy absorption characteristics. It is ideal for modelling and crafting. A comparative study of similar material was done and based on our requirements balsa was preferred.

Table 4.3 comparative study of materials

MECHANICAL PROPERTIES	BALSA	DEPRON	UNITS
Compressive strength	7	0.10	MPa
Density	13	1.56	g/cm ³
Tensile strength	14	0.7	MPa
Elongation at break	1.2	9	%
Shear modulus	0.23	8.3	GPa
Elastic modulus	3	3.5	GPa
Dielectric strength	4.9	3.7	kV/mm
Strength to weight ratio	108	98	kN-m/kg
Thermal conductivity	0.1	0.0297	W/m-K

4.4 COMPONENT SELECTION

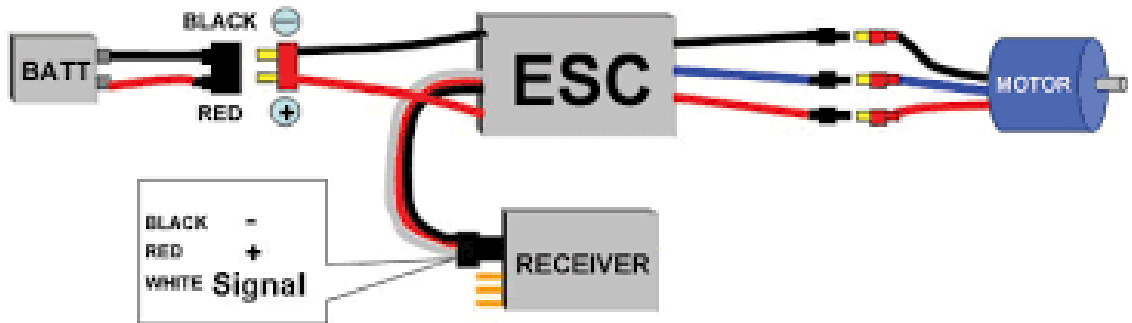


Figure 4.14 Electronics

4.4.1 MOTOR

Power plant of system is a Brushless DC Motor specially selected due to its highest efficiency among the class of DC motors. A comparative study of various brushless motors have been done depending upon our requirements.

Table 4.4 comparative study of various brushless motors

Motor	Power (watt)	Current (amp)	Kv (rpm/volt)	Weight (grams)	Thrust (N)	Propeller (inch)
N3548, 1100Kv	920	50	1100	176	21.58	12x4.5
Turnigy D3548/4 1100KV	910	50	1100	159	21.09	12X4.5
Avionic 3548 / 900KV	400	40	900	149	22.00	12x6.5
Turnigy 4240 1300KV	1300	60	1300	134	23.54	10x5
SUNNYSKY X2820	544	49.5	1100	140	25.50	14x7
Uranus 35425	506	60	1,100	150	20.60	13x6.5

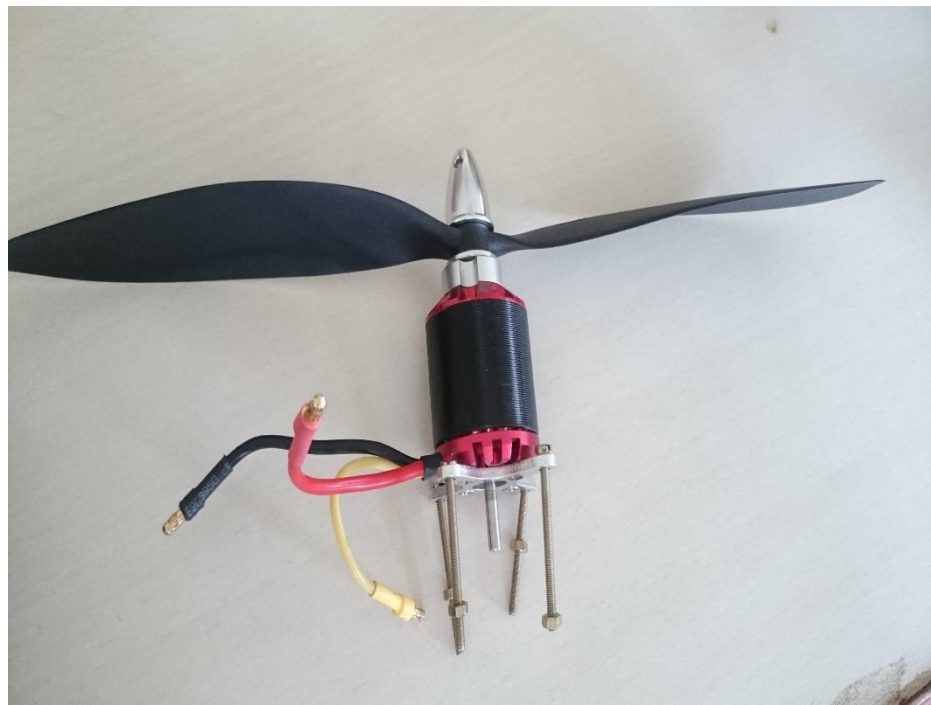


Figure 4.15 Avionic 3548 900- brushless motor

Trade-off shows Avionic 3548 900 and Turnigy D3548/1100kv motors are most suitable motors giving more thrust than required which ensures factor of safety. These motors are specifically designed to get the maximum torque at the most optimal RPM and are made for RC controlled models. The Avionic 3548 900 motor has been finally selected.

4.4.2 ELECTRONIC SPEED CONTROLLER

Electronic speed controllers are accountable for rotating the motors at the speed requested by the autopilot. Most ESCs need to know the minimum and maximum pwm values that the flight controller send for which it has to be calibrated. The ESC selected is avionic 40A



Figure 4.16 40A ESC

4.4.3 SERVOS

Tiny and lightweight with high output power. Servo can rotate approximately 180 degrees (90 in each direction), and works just like the standard kinds but smaller. Any servo code, hardware or library can be used to control these servos. It comes with a 3 horns (arms) and hardware.

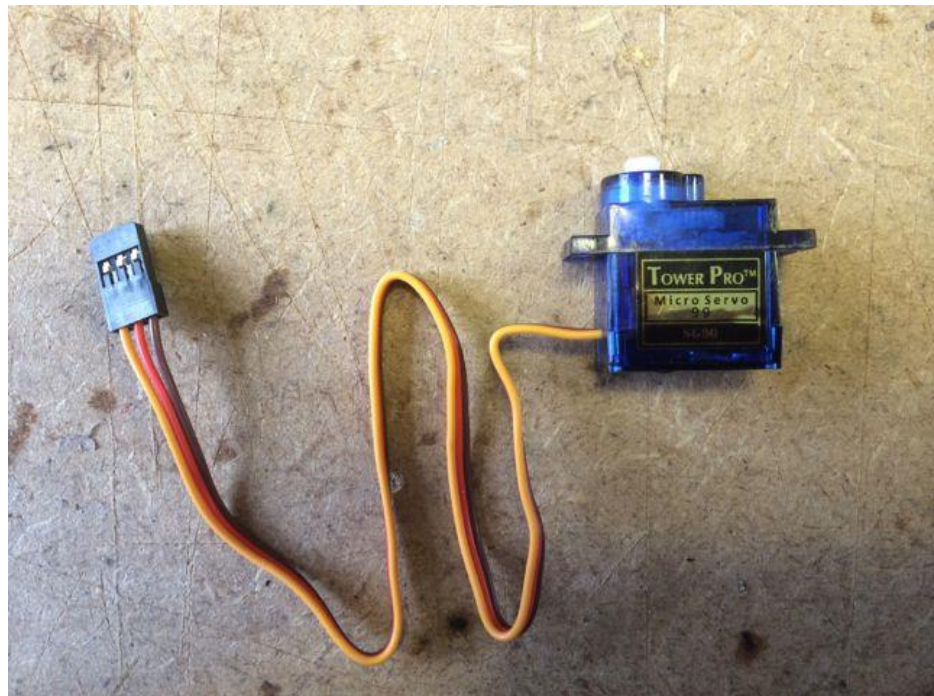


Figure 4.17 9g Servo

Table 4.5 Servo Specifications

PARAMETER	VALUE	UNITS
Dimension	22.2 x 11.8 x 31	Mm
Stall torque	1.8	kgf·cm
Operating speed	0.1	s/60 degree
Operating voltage	4.8	V
Dead band width	10	µs
Weight	9	grams

4.4.4 BATTERY SELECTION

Turnigy 3300mAh 3S 30C Li-Po Pack

Table 4.6 Battery Specification

Capacity(mAh)	3300
Config (s)	3
Discharge (c)	30
Weight (g)	297
Max Charge Rate (C)	2
Length-A(mm)	137
Height-B(mm)	43
Width-C(mm)	22

CHAPTER 5

THE UAV AUTOPILOT SYSTEM

5.1 INTRODUCTION

An autopilot is used to stabilize and control trajectory of UAV. Microcontroller is brain of Flight computer system which takes current position input from orientation and similar sensors and provides appropriate signal to actuators according to algorithm installed in it. It also transmits and receive data from ground station. Fig shows block diagram of UAS System.

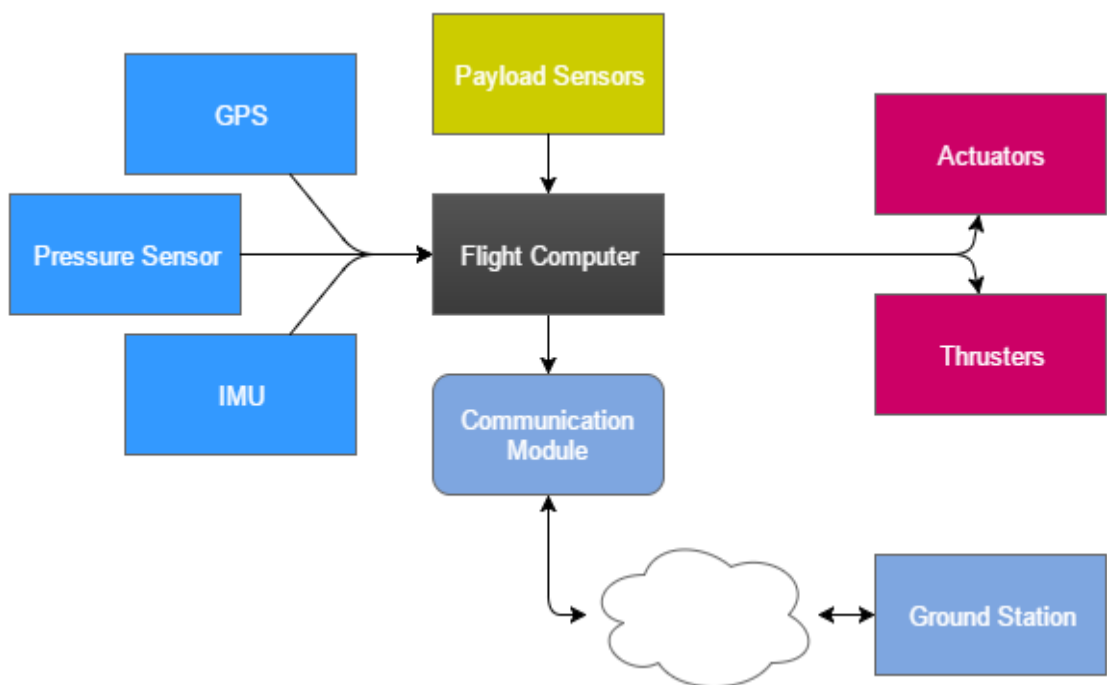


Figure 5.1 UAS System

5.2 THE FLIGHT COMPUTER

The deep space maneuver and stable altitude maintenance of an aircraft, copter or UAV is executed by a flight computer. The flight computers are operated via software programs which guide the UAVs to follow a desired flight path. The flight computer is the crux of the avionics system that enables the autonomous flight of a UAV. A control algorithm is written for the flight computer that interprets the sensor data.

For our Spherical VTOL UAV, a variety of on-board sensors are used due to its available performance and aggressive maneuvering. The on-board sensors include the accelerometer, gyroscope, pressure sensor and a magnetometer. These sensors typically guide, navigate and control the UAV.

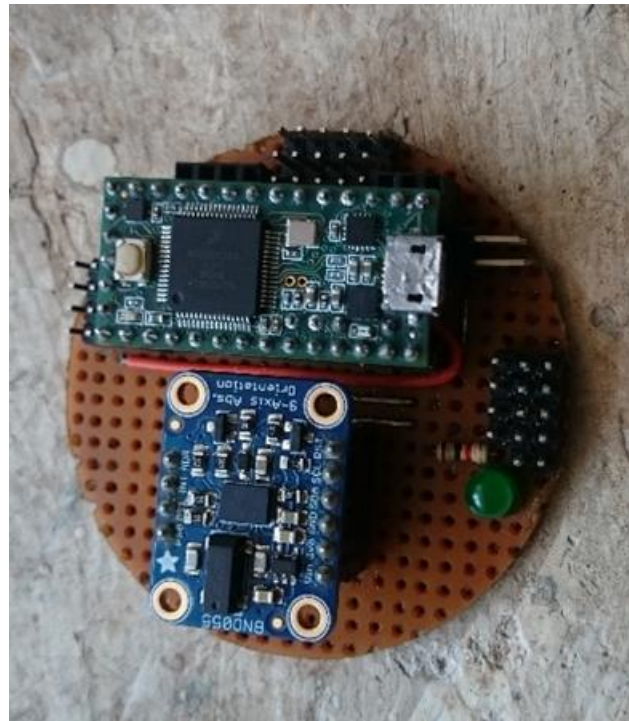


Figure 5.2 In-house designed Flight computer.

The data from the flight computer are linked to the ground station which displays the UAV's status.

5.2.1 MICROCONTROLLER

Challenge was to develop a flight computer in house which suites the requirements of project. Teensy 3.2 development board has been selected for its small size, simplicity and speed and price. It has Freescale MK20D 32bit ARM Microcontroller running at 96MHz, which is 6 times faster than conventional 8bit APM Autopilot. Also it has simple and sophisticated development tool chain, it can be programmed using Arduino IDE.

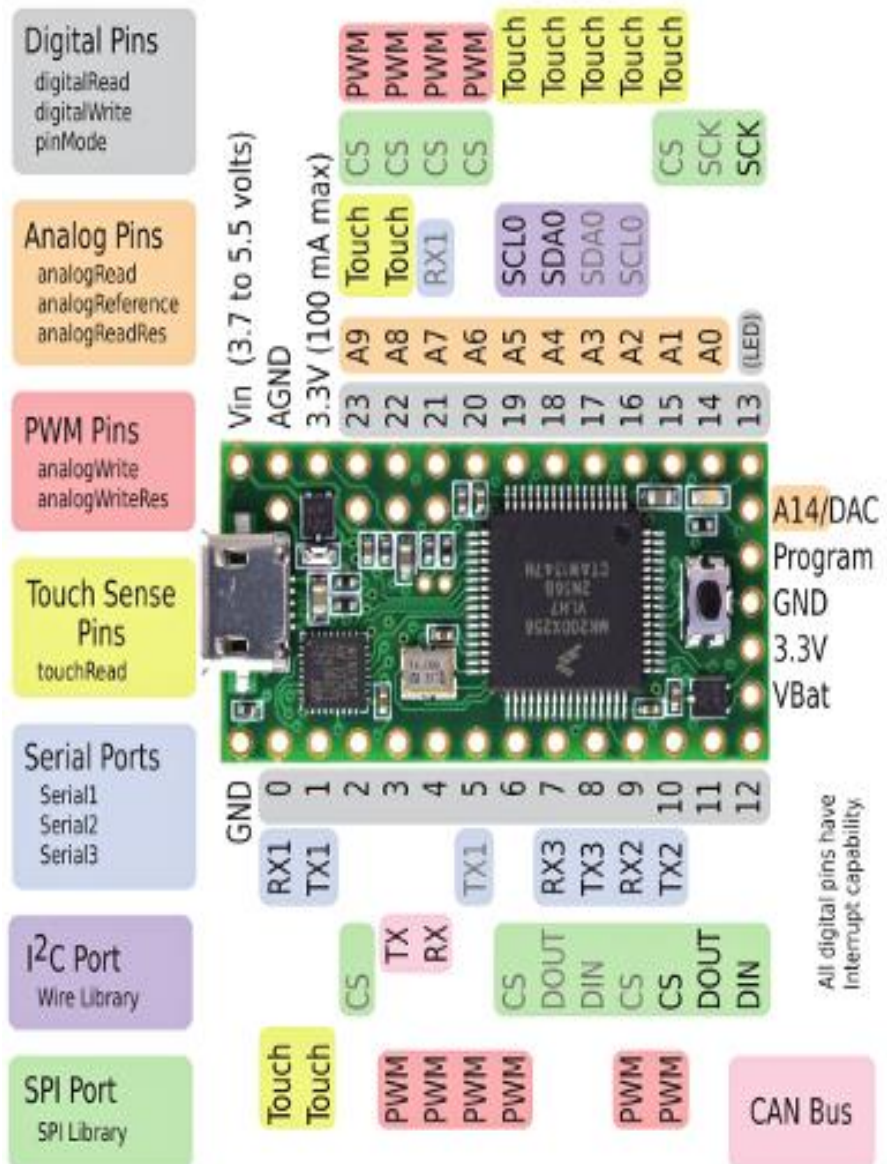


Figure 5.3 Teensy 3.2 Pin out diagram.

Table 5.1 Teensy Specifications

Feature	Teensy 3.2	Units
Processor Core Rated Speed Overclockable	MK20DX256VLH7 Cortex-M4 72 96	MHz MHz
Flash Memory Bandwidth Cache	256 192 256	kbytes Mbytes/sec Bytes
RAM	64	kbytes
EEPROM	2	kbytes
Direct Memory Access	16	Channels
Digital I/O Voltage Output	34 3.3V	Pins Volts
Analog Input Converters Resolution Usable Prog Gain Amp Touch Sensing	21 2 16 13 2 12	Pins Bits Bits Pins
Analog Output DAC Resolution	1 12	Pins Bits
Timers FTM Type PWM Outputs	12 Total 3 12	Pins
Communication USB Serial With FIFOs High Res Baud I2C CAN Bus	1 3 2 3 2 1	

5.2.2 BAROMETRIC SENSOR

It is necessary to know the exact position of a UAV problems related to the balancing of the UAV occur at higher altitude with varying velocity and pressure. A pressure sensor is used as an option to measure the exact co-ordinates of a UAV. As the atmospheric pressure decreases with increase in altitude, it follows the equation:

$$h = \frac{T_0}{T} \times \left(1 - \left(\frac{P}{P_0} \right)^{\frac{R}{g}} \right)$$

Where T is the temperature, T_0 is the temperature at sea level, P_0 is the pressure at sea level, P is the pressure at altitude h. The pressure sensor using the altitude h.

The two pressure sensors considered for our requirements are: BMP180 which offers a pressure measuring range of 300 to 1100 hPa with an accuracy down to 0.02 hPa in advanced resolution mode. It's based on piezo-resistive technology for high accuracy, ruggedness and long term stability. The chip only accepts 1.8V to 3.6V input voltage and MS5611 which is a high precision pressure sensor module and includes a linear pressure measurement and an ultra-low power. The MS5611 provides different operation modes that allow optimizing for speed and current consumption. The pressure sensor BMP180 has been selected due to its availability and low cost.

Table 5.2 BMP180 Specifications

Item	Min	Typical	Max	Unit
Voltage	3	5	5.5	VDC
Current	1.1	/	20	uA
Pressure Range	300	/	1100	hPa
Faster I2C data transfer	/	/	3.4	MHZ
Dimension	40.1*20.2*9.7			mm

5.2.3 IMU

The IMU is a single unit in the electronics module which collects angular velocity and linear acceleration data which is sent to the main processor. The IMU or Inertial Measurement Unit is a sensor that hosts two types of sensors. The accelerometer sensor measure acceleration in two different units including meters per second squared, or when the acceleration felt like a weight, in G-forces. Inside this tiny sensor is a small system that bends when a momentum or gravity force is applied. The amount of bend has a proportional value of the output signal. The advantages of the accelerometer sensor include a high accuracy in applications with noises, as well the acceleration measurement down to zero Hertz. The biggest disadvantage of this sensor is the limited high frequency where the sensor works.

The gyroscope sensor is inexpensive and measures in degrees per second or revolutions per second the angular velocity. It's frequently used in robotic applications to measure the balancing and send corrections to motors or drones to stabilize the flight. This tiny sensor uses a disc with a large heavy rim designed to resist movement when is spinning on its axis.

To estimate position orientation of system 9 axis Inertial Measurement Unit is used, which includes 3-axis Accelerometer, 3-axis Gyroscope and 3 axis Magnetometer. Data from all these sensor is gathered and converted to Euler angles (Roll, Pitch, Yaw).

An inertial measurement unit is an electronic device which uses a conjunction of accelerometers, magnetometers and gyroscopes to measure the body's linear motion, angular motion and the magnetic field around the body. It helps in the maneuvering of an unmanned aerial vehicles and is the main component of the navigation system. It works by detecting the current rate of acceleration using accelerometers, and detects changes in rotational attributes like pitch, roll and yaw using one or more gyroscopes. The magnetometer mostly assists calibration against orientation drift.

The BNO-055 is a 9-axis motion sensor. The BNO-055 has an embedded Cortex M0 ARM processor as well as accelerometer, gyroscope and magnetometer for a purely hardware absolute orientation solution. The first of the inexpensive embedded sensor fusion motion sensors was the 6-axis MPU6050 by Invensense, and the latest Invensense 9-axis motion sensor the MPU9250 maintains the technology with the

Digital Motion Processor or DMP providing 6-axis sensor fusion. The drawback of Invensense's approach is the microprocessor must upload a large (4K) binary file of firmware for the DMP, and the DMP is still limited to 6-axis sensor fusion despite being embedded in a 9-axis motion sensor. This device requires no binary firmware and the quaternion or heading results of the sensor fusion are read from the MAX21100 registers like any other data. Also in this class is the EM7180, which is a sensor fusion hub that takes data from external sensors and performs sensor fusion in hardware for readout by a master microcontroller.

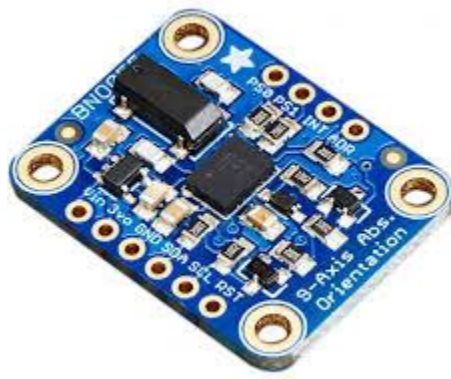


Figure 5.4 BNO 055 9-Axis IMU

The latest class of integrated motion sensor is embodied in the BNO-055. In this device the 9-axis motion sensor (the BMX-055) coupled with a Cortex M0 ARM processor to perform the 9-axis sensor fusion. No external magnetometer and no microcontroller processing is required; again the quaternions, linear acceleration, gravity vector, and heading information are directly readable from the BNO-055 registers.

The reason BNO-055 has been selected because it has a lot of functions and communication paths and they are available in a small breakout board. The BNO-055 breakout board communicates via I2C (default), UART, or HID-I2C protocol. The BNO-055 breakout board also breaks out the device reset, which is triggered by setting the reset pin low.

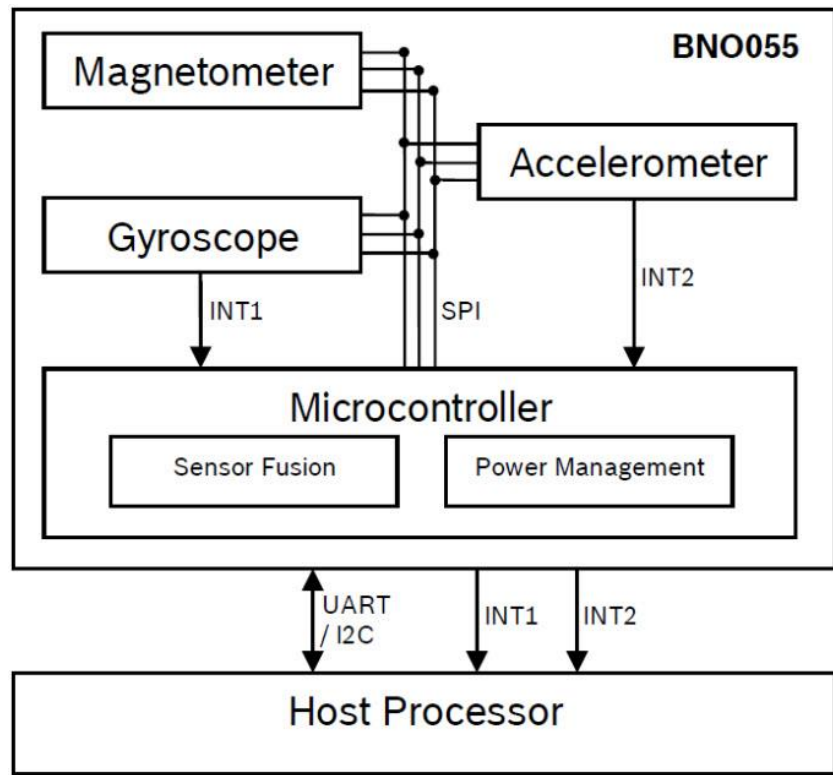


Figure 5.5 9-Axis IMU Architecture

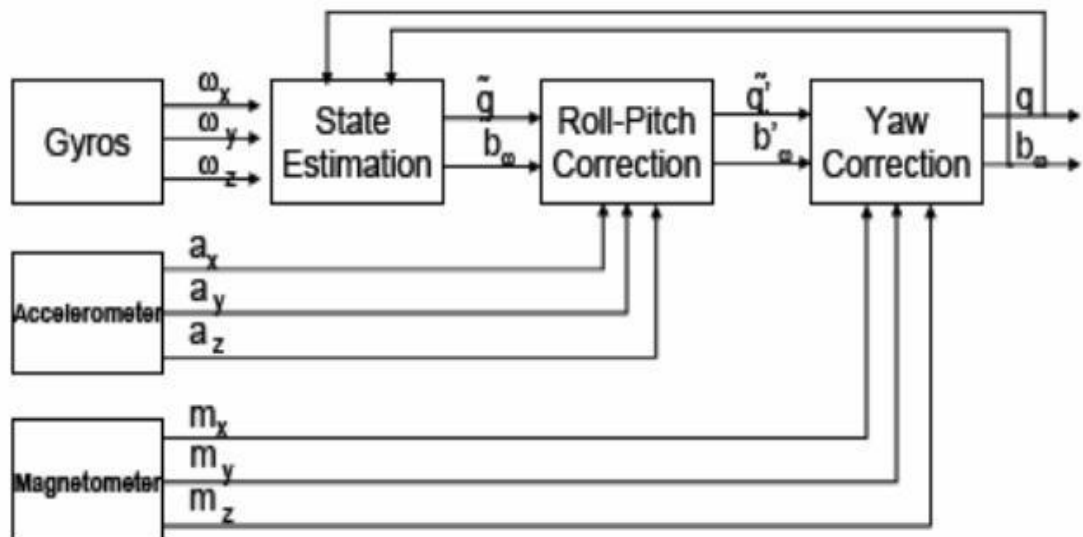


Figure 5.6 9-Axis IMU Fusion.

Data received from sensors is to be processed and inherent noise should be removed. Low pass Filter is applied to each sensor to smoothen the data, afterwards 9-axis sensor data is to be converted to Euler angles using sensor fusion.

Sensor fusion is an highly sought after research because it can decrease circuit complexity and improves compactness of the system. One of the most difficult problems faced in sensor fusion is various sensors working in different gain points in frequency domain. To solve this issue we used extended Kalman filter and Madgwick's 9 axis sensor fusion algorithm. After getting data from Sensors, orientation of the UAV is now known to the microcontroller it calculates the error and takes correction step by accordingly providing output to actuators which in this case are control surfaces and BLDC Motor.

5.2.4 STABILITY AND CONTROL ALGORITHM

Microcontroller Takes control Input such as throttle speed, roll and pitch control from various means such as RC Receiver, Bluetooth module, Xbee etc. This speed is mapped to appropriate ESC Speed.

Since this UAV is symmetric about its vertical axis and have only one rotor which produces yawing moment about its axis. To cancel this yawing moment flow from propeller is used to produce lift at control surfaces, this lift is proportional to angle of attack of control surface. Now to produce exactly equal and opposite yawing moment appropriate angle of attack is calculated.

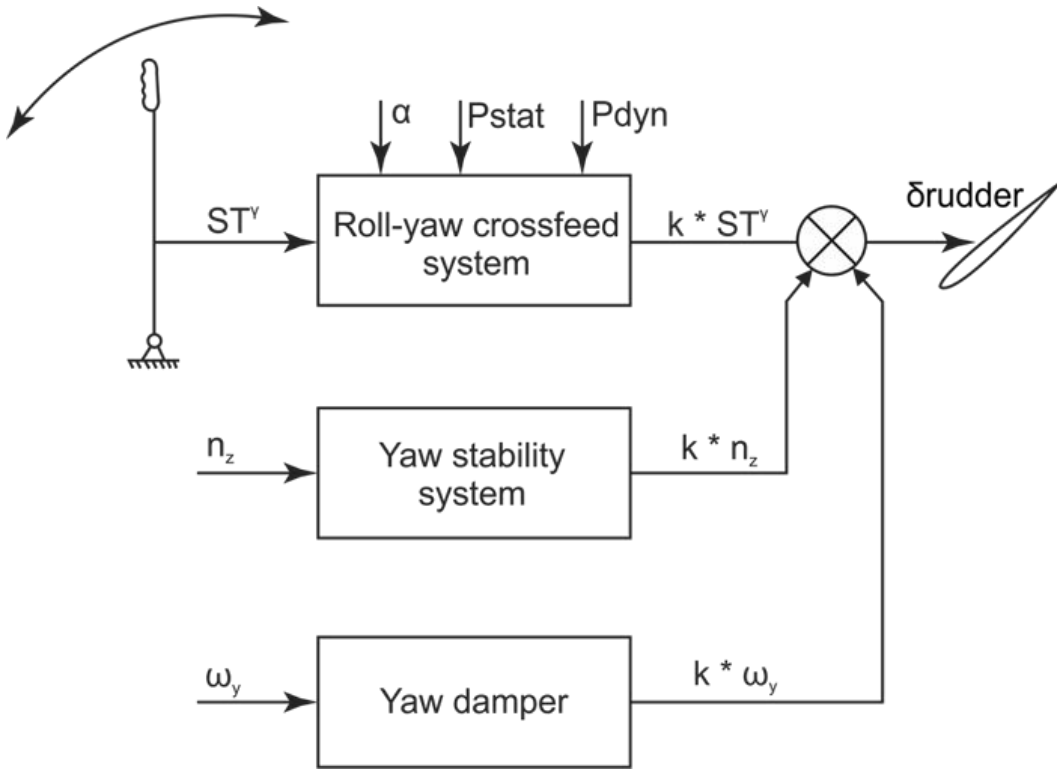


Figure 5.7 Yaw Stability algorithm.

Pitching and Rolling of system are symmetric and can be adjusted using pitch angle and roll angle to achieve desired set point.

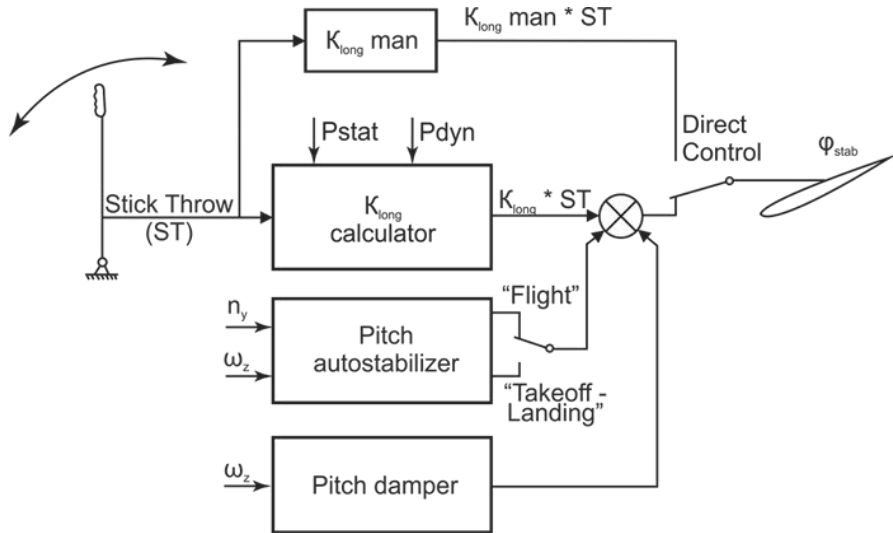


Figure 5.8 Pitch, Roll Stability algorithm

Different types of combinations are used to stabilize the system which are Rudders for Yawing and Flaps for pitching and rolling Moment, Both rudders and flaps for Yawing Pitching and rolling moment and tested accordingly.

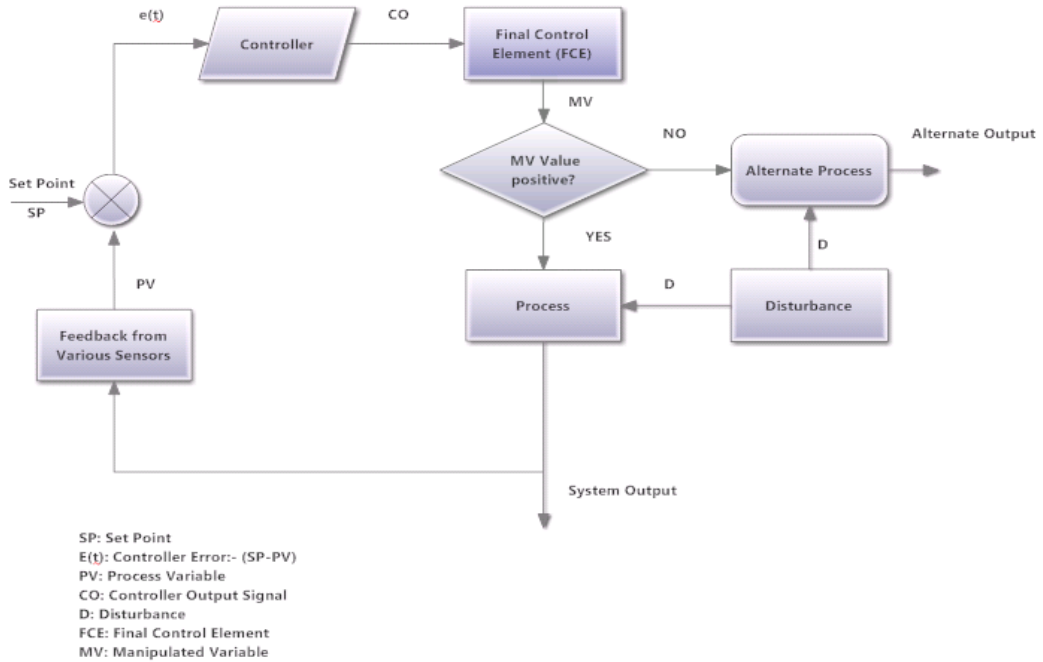


Figure 5.9 Feedback Control loop

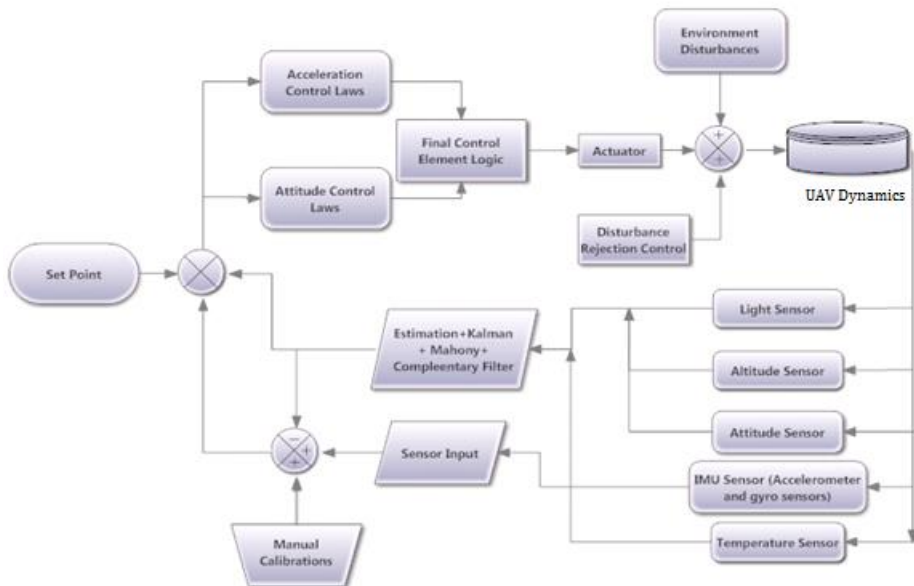


Figure 5.10 Flight Computer Block Diagram

5.3 GROUND STATION

An indigenous Ground station software is developed for data acquisition and telemetry display, which provides a nice Interface to Pilot to real-time monitor the state of UAV.

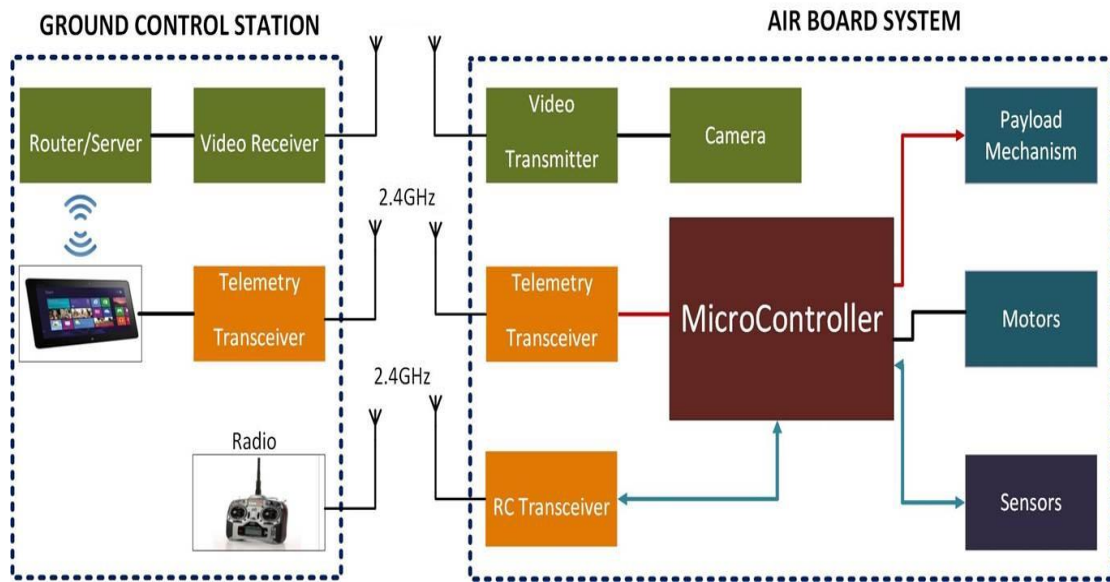


Figure 5.11 Ground Station and Flight Computer Integration Block Diagram

Ground Station is developed using Microsoft Visual Studio Interactive development Environment, C#.Net is selected as development programming language due to its support for exception handling and multithreading. Ground station consist of an Attitude and Heading Instrument Indicator, Climb rate indicator and GPS Location both online and offline.

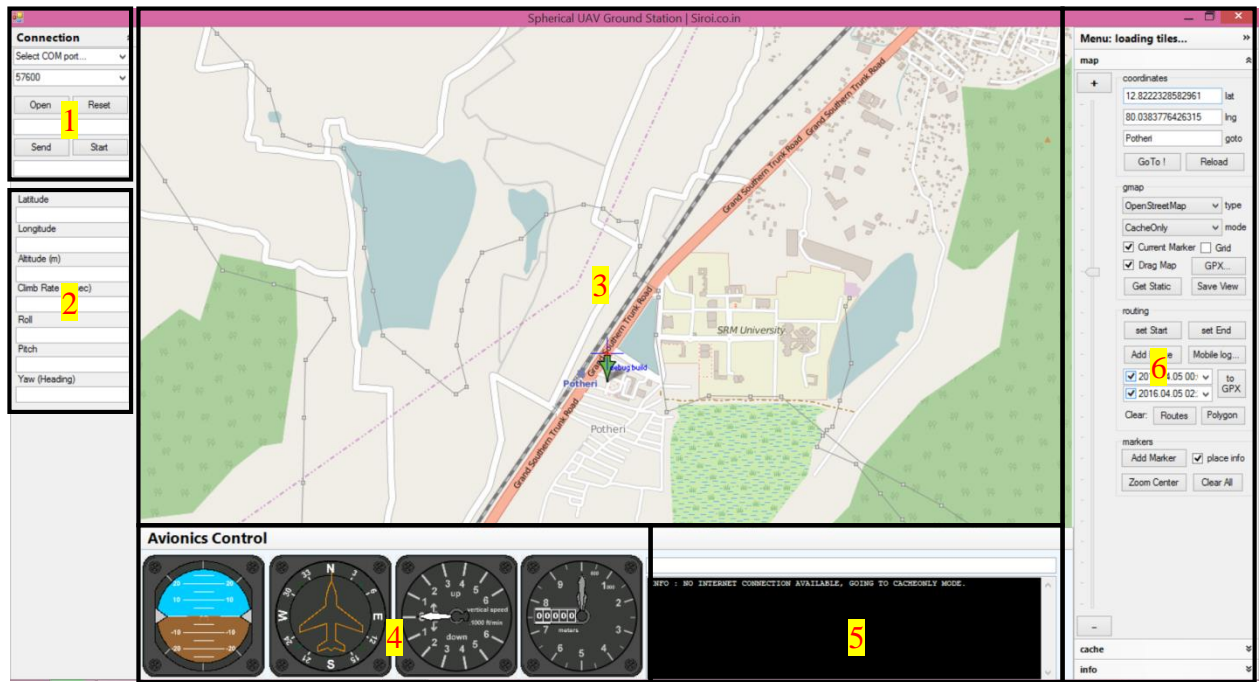


Figure 5.12 Ground Station GUI

G1UI of ground station is divided in 6 sections

1. Connection Handle: Establish connection with UART port.
2. Sensor Field : display current sensor data in text field
3. Map : Displays current position of UAV
4. Avionics Instrument Panel consists of Attitude Indicator, Heading Indicator, Vertical Speed Meter and Altimeter
5. Debug Log
6. Map Control : Modify Map parameters



Figure 5.13 Avionics Instrument Panel

5.4 COMMUNICATION AND DATA HANDLING

Large data to be sent from UAV to Ground station and manual remote control, since data rate of communication module is limited an efficient method is to be develop to handle packets of data. Also integrity of data is major factor. Data to be sent from UAV to ground station is attitude and heading and position of system of system with payload sensor data given as follows.

- Roll
- Pitch
- Heading
- Latitude, Longitude
- Altitude
- Climb rate
- Payload Sensors

RF UART Transceiver module is mounted on both UAV and Ground Station.



Figure 5.14 XBEE Pro Series 2

XBEE 2.4 GHZ RF UART Module is selected for Half Duplex Communication because of better power output and data protocol of the pro series 2.

XBEE Specifications

- 2.4 GHz with duct antenna
- 250 kbps data rate

- 50 mW output
- 1 mile range
- 6 10-bit ADC input pins
- 8 digital IO pins
- 128-bit encryption
- Operating at 3.3 V@295mA

To minimize data loss and ensure successful duplex communication data is first encrypted to base 64 number system, which is minimizing the size of packet

Since large amount of data such as Roll, Pitch, Heading, GPS co-ordinates, etc.. is to be sent from UAV to ground station and vice versa XBEE 2.4 GHz module is used. To make sure data is sent without error at high data rate it is compressed to smaller base 64 string before sending and decoded at receiving end.

Data Packet format <Roll>,<Pitch>,<Heading>,<Lat>,<Long> is converted as **#oooooo**; each **oo** bit varies from 0 to 4095. '#' is start code of packet and ';' stop code of packet.

5.6 ELECTRICAL POWER SYSTEM

Different Electronic equipment, sensors and actuators has different power requirement hence proper voltage and current should be given. Which is achieved using small size 3A DC to DC buck convertor.

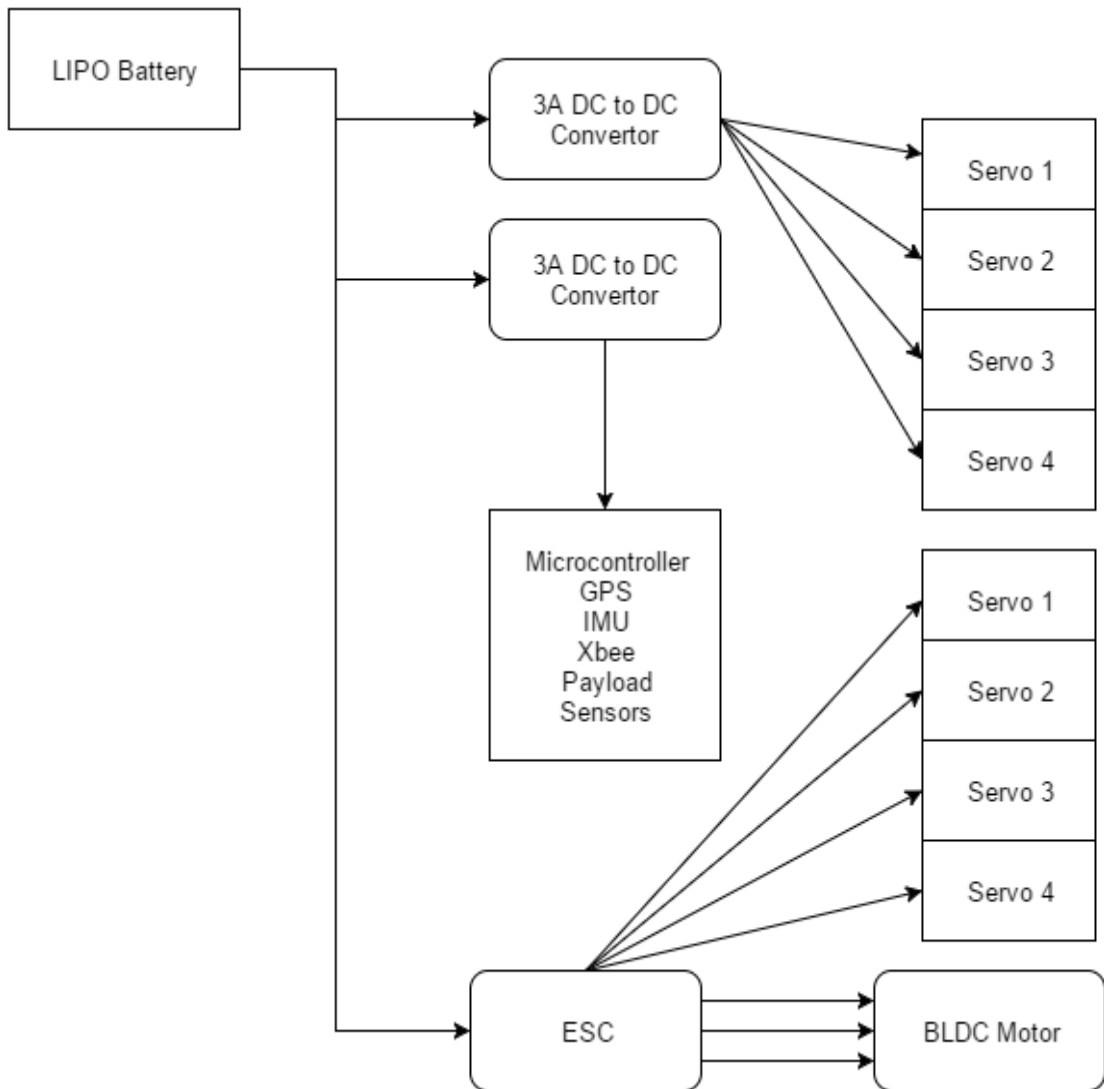


Figure 5.15 Electrical Power System.

5.6.1 3A MINI DC TO DC CONVERTER

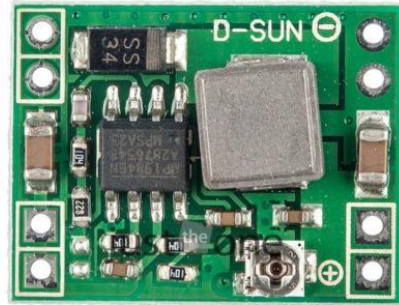


Figure 5.16 DC to DC Converter

Description

- i. Module Properties: Non-isolated step-down module (BUCK)
- ii. Rectification: Synchronous rectification
- iii. Input voltage: DC 4.75V-23V
- iv. Output voltage: DC 1.0V-17V (Adjustable, Output < Input)
- v. Output current: Rated current 1.8A (3A MAX, can not be prolonged)
- vi. Conversion efficiency: 96% (highest)
- vii. Switching Frequency: 340KHz.
- viii. Output ripple: 30mV (no-load)
- ix. Load regulation: $\pm 0.5\%$
- x. Voltage regulation: $\pm 2.5\%$
- xi. Operating Temperature: Industrial (-40° ~ +85°)
- xii. Short circuit protection: No (Please do not short-circuit)
- xiii. Input Reverse protection: No (Cannot be reversed)
- xiv. 22mm * 17mm * 4mm (L * W * H) / 0.87" * 0.67" * 0.16" approx. Super mini board

CHAPTER 6

ANALYSIS

6.1 INTRODUCTION TO ANSYS

ANSYS provides a comprehensive suite of computational fluid dynamics software for modelling fluid flow and other related physical phenomena. It offers unparalleled fluid flow analysis capabilities, providing all the tools needed to design and optimize new fluids equipment and to troubleshoot existing installations. The primary ANSYS products in the fluids area are ANSYS Fluent and ANSYS CFX. With these solutions you can simulate a wide range of phenomena: aerodynamics, combustion, hydrodynamics, mixtures of liquids/solids/gas, particle dispersions, reacting flows, heat transfer, and much more. Steady-state and transient flow phenomena are easily and quickly solved.

The graphic results of an ANSYS CFX or ANSYS FLUENT CFD software simulation will show you how fluid flow, particle flow, heat transfer, chemical reactions, combustion, and other parameters evolve with time.

ANSYS CFX and ANSYS FLUENT CFD software are also available together in the ANSYS CFD bundle. With ANSYS CFD software, you have access to an unprecedented array of fluid flow physics models, allowing you to analyse your equipment with a great deal of confidence. ANSYS CFD technology is highly-scalable, allowing for efficient parallel calculations on thousands of processing cores.

Flow over different geometry is studied using ANSYS Fluent at different velocities and angle of attack to get idea of locations where eddies formed in flow.

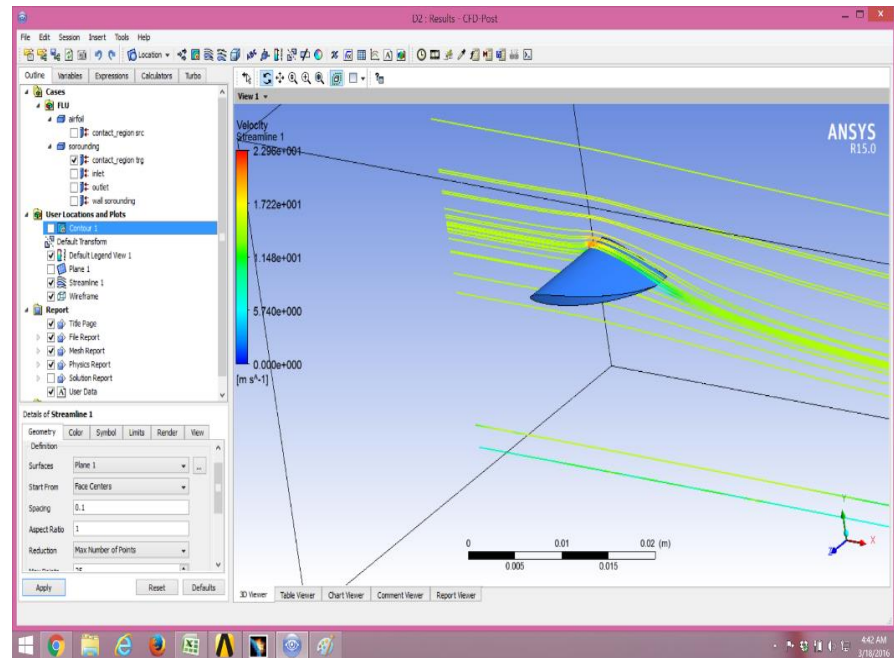


Figure 6.1 3D Streamline Flow over rudder

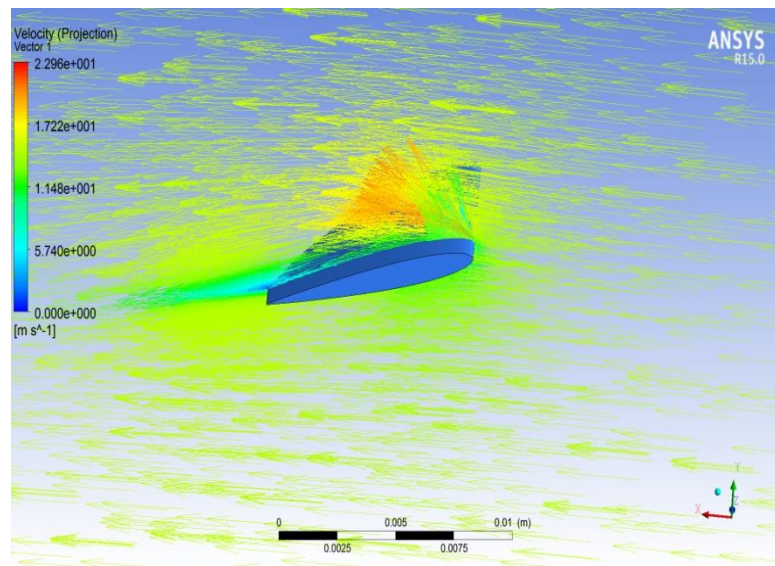


Figure 6.2 Velocity vectors over rudder

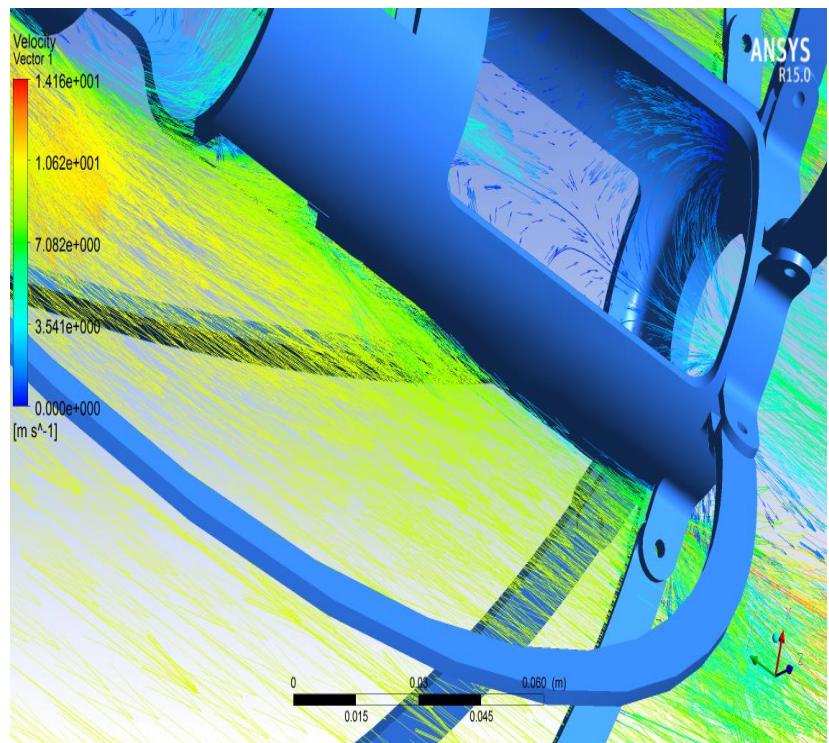


Figure 6.3 3D Flow visualisation over body

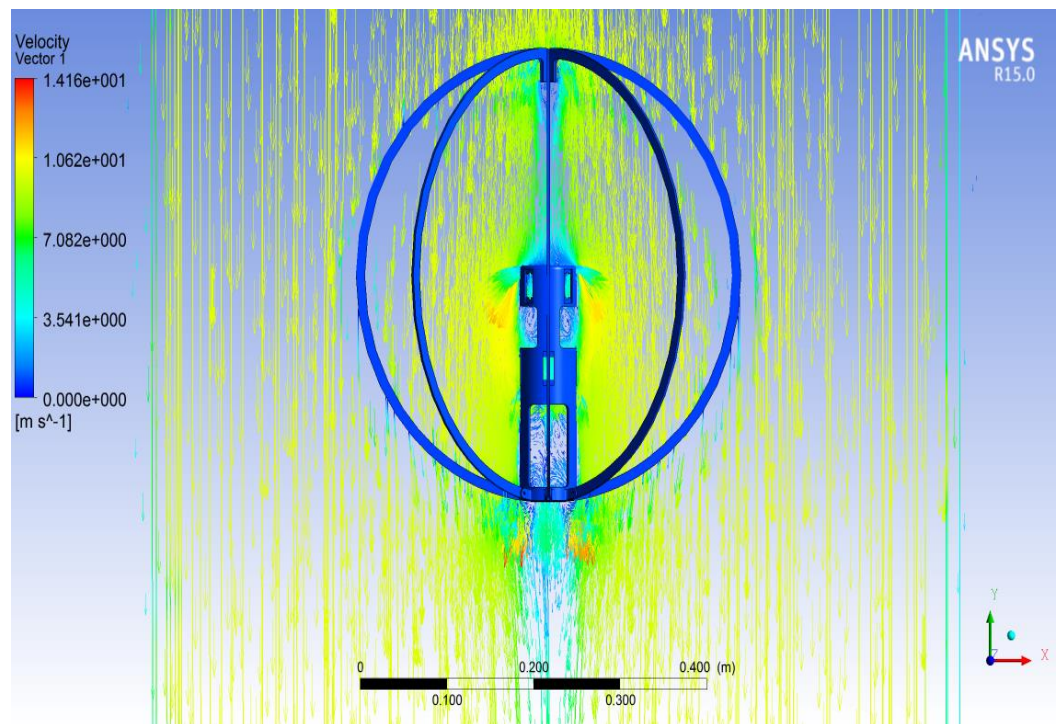


Figure 6.4 3D Flow visualisation over body

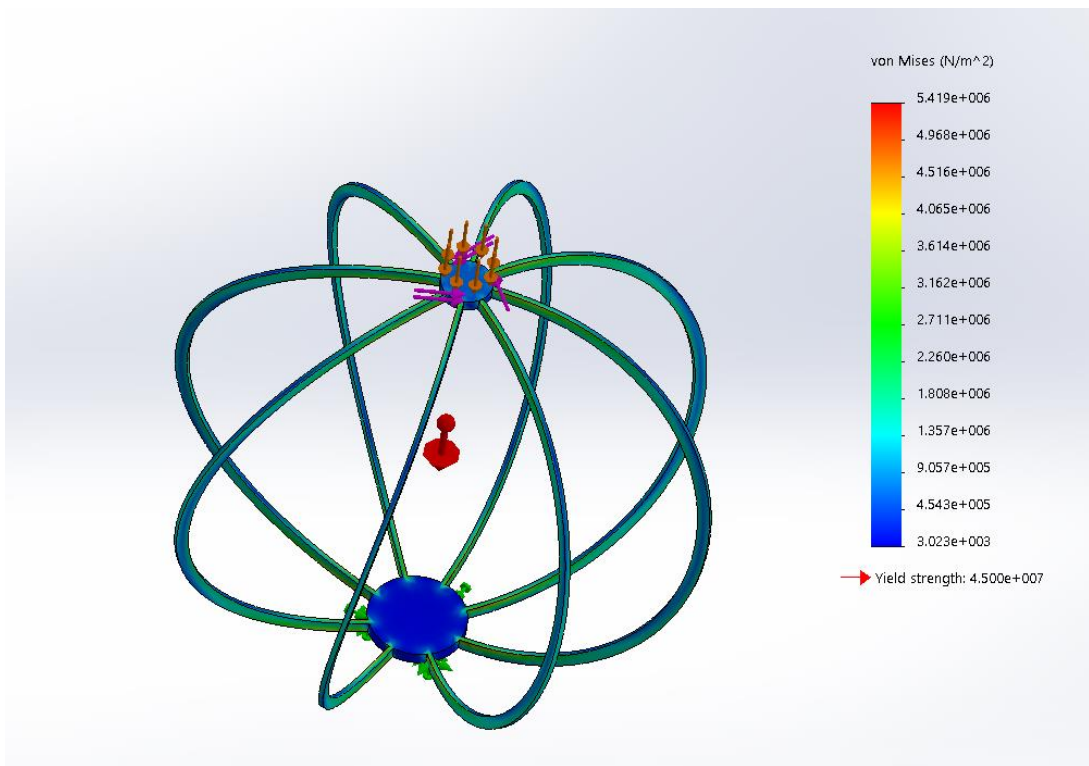


Fig 6.5 Visualisation of Stress magnitude.

CHAPTER 7

FABRICATION

7.1 ALUMINIUM SPARS FABRICATION

The aluminium spars of the model were fabricated using Wire EDM machining (Electrical Discharge Machining) which is an electro thermal production process in which a thin single-strand metal wire in conjunction with de-ionized water (used to conduct electricity) allows the wire to cut through metal by the use of heat from electrical sparks. Due to the inherent properties of the process, wire EDM can easily machine complex parts and precision components out of hard conductive materials.



Figure 7.1 Aluminium sheet

7.2 CORE BODY – ABS-M30

The 3D printing technology has been used to fabricate the core body, also known as additive manufacturing, turns digital 3D models into solid objects by building them up in layers. 3D printing encompasses a wide range of additive manufacturing technologies. Each of these builds objects in successive layers that are typically about 0.1 mm thin. The methods used vary significantly, but all start with a computer aided design (CAD) model or a digital scan. This is then processed by 'slicing software' that divides the object into thin cross sections that are printed out one on top of the other. The body was fabricated at the SRM RPT lab using ABS-M30 material. It was fabricated in about 22 hours including the cleaning process.



Figure 7.2 3D Printed core body



Figure 7.3 On-Going cleaning process at SRM RPT Lab

7.3 CONTROL SURFACES – BALSA

The control surfaces were manually fabricated from Balsa sheets of dimensions 3mm x 10mm x 1000mm.

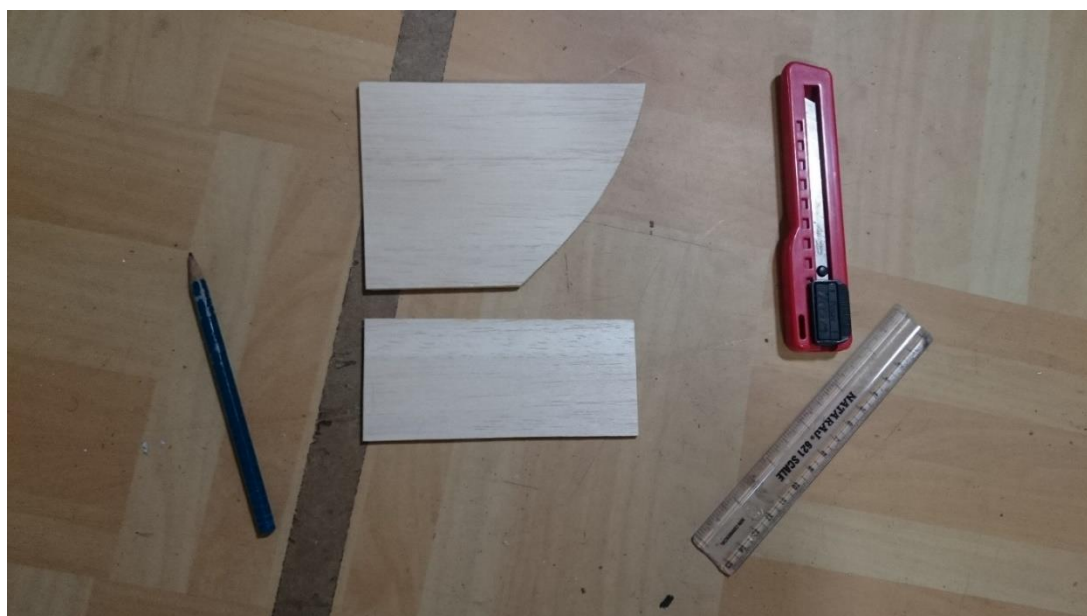


Figure 7.4 In-house fabricated control surfaces

CHAPTER 8

TESTING AND EXPERIMENTAL SETUP

This Experimental Setup chapter contains descriptions of the experimental plan, test specimen geometry and material properties and sensor properties of the several tests performed on the model.

8.1. SENSORS TEST

The BNO5 was tested using the sensor fusion algorithm. The accelerometer, magnetometer and gyroscope were tested and verified. The values of Euler angles, rotation vector, and heading and quaternion angles were established.

8.2. MOTOR AND SERVO TEST

The motor and servos were tested, at varying RPM and angles respectively, using a Microcontroller. The angles for all the eight servos were calibrated.

8.3. TRANSLATORY AND YAWING MOTION / STABILITY TEST

The test setup for the stability test consists of a pneumatic piston of stroke length 150mm and a wooden frame. The piston was mounted vertically on the side wall of the wooden box with nut and bolt. A hole was drilled at the bottom of the test prototype and was fixed to the movable end of the piston. The prototype was allowed free translational and yawing motion about the piston axis. The servos attached to the control surface are connected to the flight computer and the entire setup is being powered by 11.1V battery. The body is being supported by two wooden planks to prevent any damage due to the vibration. The entire setup is shown in the fig. 8.1



Figure 8.1 Entire setup for the test

The rpm of the motor is regulated by providing manual inputs and the angle of the control surfaces were accordingly changed to generate sufficient side force to counteract the torque created by the motor. The main aim of the experiment was to test the effectiveness of the control surfaces, motion of the body and to observe the vibration generated due to torque, the behaviour of the model at various rpm and angle of attacks of the control surfaces and the angle at which the control surfaces produces sufficient side force to counteract the torque generated by the motor to attain stability.

The test concluded with the observation of translational motion and yawing of the model. It was inferred that at an angle of attack of 15 degree at 50 percent throttle stability was attained due to the control surfaces.

8.4. SIX COMPONENT BALANCE TEST

The measurement of the forces acting on a body moving in air, required to analyse the aerodynamic characteristics of the uav, is measured using a six component balance equipment as shown in the Fig. 8.2



Figure 8.2 six component balance setup

The model is mounted on the stem that protrudes in to the test section and has a simple mechanism for pitching and yawing the model. The stem is fixed on a metric plate which transfers the loads on to 6 Strain elements. The outputs from the Strain gauge mounted on the strain elements are amplified by appropriately designed amplifiers. These signal conditioners amplifiers are designed using low noise and highly stable instrumentation amplifiers. The outputs from these amplifiers are measured using a microcontroller based measurement system. The measurement system has a keyboard

and a display which are useful in setting up the system and displaying the data from the instrumentation amplifiers. The entire setup is shown in the fig. 8.3

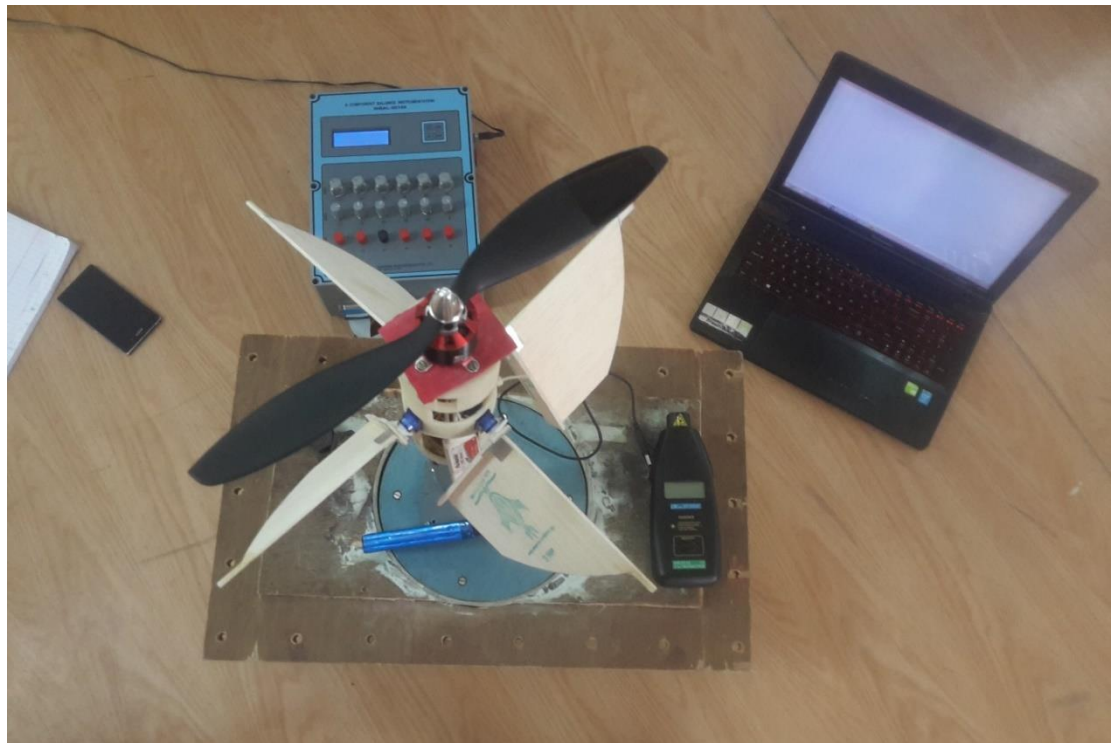


Figure 8.3 Entire setup for 6 component balance test

The model was mounted on the balance, the incidence angle of the model was set to zero and the screws were tightened. An averaging interval of $_$ was set. The wind off mode had been selected under the Data mode. The voltages v1, v2, v3, v4, v5 and v6 values had been tuned to zero.



Figure 8.4 Calibration of voltage

The values of lift, pitching moment, rolling moment, side force, yawing moment and drag were noted in the wind off mode. The steps were repeated for different rpms and angle of attack of the control surfaces. The outputs V_1, V_2, V_3, V_4, V_5 and V_6 are related to L, P_m, R_m, S_F, D , and Y_m .

CHAPTER 9

TEST RESULTS AND CONCLUSION

9.1 SIX COMPONENT TEST

Results showed in 6 component balance sates that yawing moment of single rotor can be stabilised and control surfaces are effective enough to produce counter torque generated by motor. Practically system is tethered to cable from top and controlled tested completely on autopilot system which is capable of making the UAV stable in yawing moment.

Table 9.1 SIX Component Test Results

CONDITIONS	Time	Lift	Drag	Side Force	Pm	Rm	Ym
	seconds	Kg	Kg	Kg	kg-cm	kg-cm	kg-cm
$\alpha = 0^\circ$	10	-0.008	0	-0.004	0.052	0.399	0.016
Rpm = 0	20	-0.005	0.002	-0.002	0.046	0.434	0.012
propeller off	30	-0.004	-0.008	-0.006	-0.004	0.275	0.014
	50	0.011	-0.011	-0.005	0.033	0.782	0.018
	60	0.013	-0.008	-0.004	0.056	0.564	0.016
	80	0.004	-0.012	-0.002	0.032	0.667	0.011
	100	-0.004	-0.011	-0.003	-0.003	0.421	0.009
	120	0.013	-0.008	0.001	0.022	0.387	0.025
	140	-0.005	-0.007	0.002	0.059	0.678	0.015
	180	0.012	-0.011	-0.004	0.049	0.276	0.022
Average		0.0027	-0.0074	-0.0027	0.0342	0.4883	0.0158

Table 9.2 SIX Component Test Results

CONDITIONS	Time	Lift	Drag	Side Force	Pm	Rm	Ym
	seconds	Kg	Kg	Kg	kg-cm	kg-cm	kg-cm
$\alpha = 0^\circ$	10	0.177	-0.012	0.026	-0.559	-0.81	-0.172
Rpm = 3300	20	0.189	-0.011	0.033	-0.549	-0.71	-0.189
propeller on	30	0.213	-0.006	0.036	-0.57	-0.65	-0.164
	60	0.156	0.002	0.015	-0.569	-0.95	-0.178
	80	0.132	0.006	0.019	-0.544	-0.77	-0.182
	100	0.176	0.009	0.021	-0.55	-0.72	-0.165
	120	0.219	-0.013	0.029	-0.601	-0.83	-0.179
	140	0.229	0.01	0.03	-0.551	-0.69	-0.188
	180	0.166	0.007	0.037	-0.541	-0.88	-0.176
Average		0.149	0.011	0.017	-0.61	-0.61	-0.173

Table 9.3 SIX Component Test Results

CONDITIONS	Time	Lift	Drag	Side Force	Pm	Rm	Ym
	seconds	Kg	Kg	Kg	kg-cm	kg-cm	kg-cm
$\alpha = 15^\circ$							
Rpm = 4300	10	0.328	-0.019	0.028	-0.36	0.447	-0.032
propeller on	20	0.336	-0.016	0.022	-0.31	0.412	-0.03
	30	0.342	-0.021	0.033	-0.29	0.456	-0.029
	60	0.39	-0.014	0.036	-0.42	0.466	-0.022
	80	0.31	-0.015	0.021	-0.45	0.442	-0.02
	100	0.33	-0.017	0.026	-0.39	0.436	-0.027
	120	0.329	-0.022	0.03	-0.28	0.437	-0.019
	140	0.316	-0.02	0.027	-0.36	0.444	-0.033
	180	0.325	-0.013	0.024	-0.35	0.44	-0.023
Average		0.332	-0.023	0.027	-0.37	0.439	-0.019

Table 9.4 SIX Component Test Results

CONDITIONS	Time	Lift	Drag	Side Force	Pm	Rm	Ym
	seconds	Kg	Kg	Kg	kg-cm	kg-cm	kg-cm
$\alpha = 30^\circ$	10	0.664	0.001	0.05	-1.773	0.018	2.606
Rpm = 4300	20	0.662	-0.002	0.06	-1.878	0.016	2.652
propeller on	30	0.659	0.003	0.063	-1.889	0.011	2.304
	60	0.66	0	0.056	-1.779	0.012	2.403
	80	0.65	0.004	0.061	-1.699	0.015	2.422
	100	0.674	0.005	0.052	-1.756	0.02	2.658
	120	0.67	-0.003	0.049	-1.742	0.021	2.647
	140	0.657	-0.002	0.055	-1.779	0.015	2.661
	180	0.665	0.002	0.062	-1.782	0.011	2.669
Average		0.6658	0.001	0.051	-1.789	0.013	2.66

The angle and rpm at which the yaw moment of the body approached zero was noted and considered as the main inference of the experiment.

Data from various test results with different angles of attack and at different rpm is taken and average value of all data gathered is used to plot final graph.

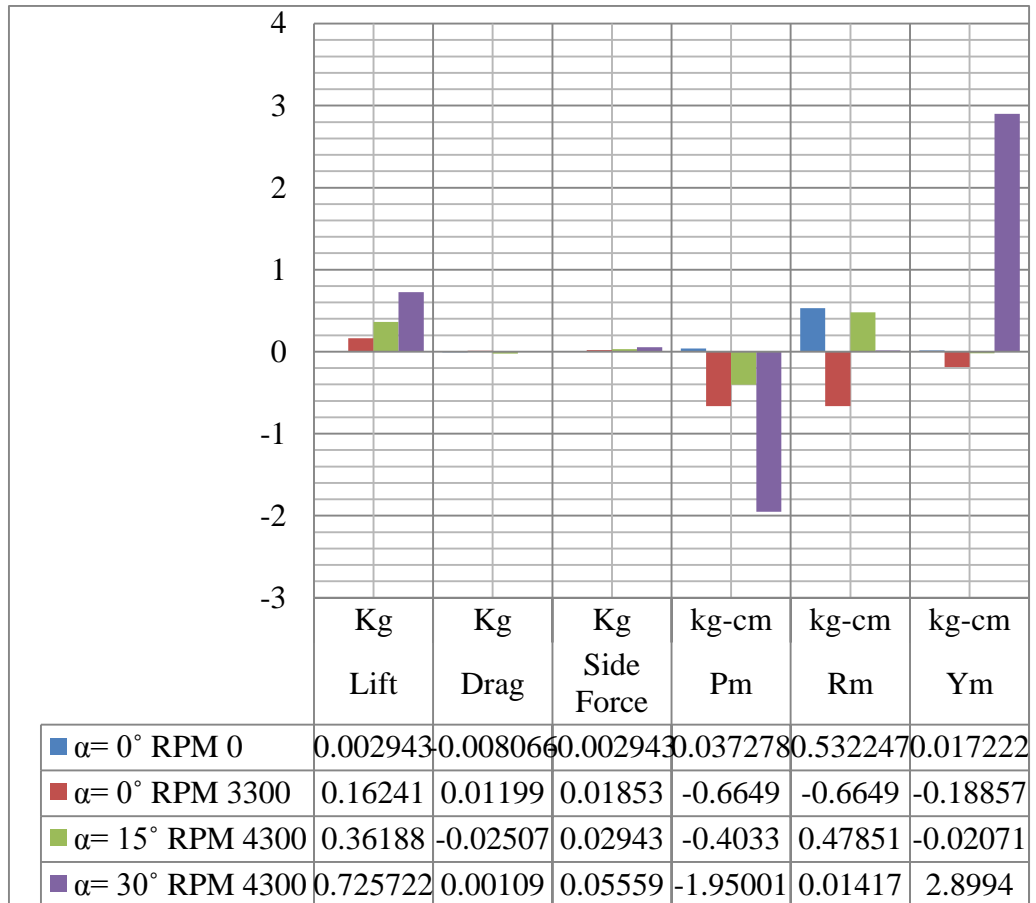


Figure 9.1 SIX Component Balance Force and Moment Graph.

9.2 GROUND STATION TEST

Data Received from UAV is verified using Serial Monitor and on Ground station text fields, further data is plotted Yaw angle vs Time.

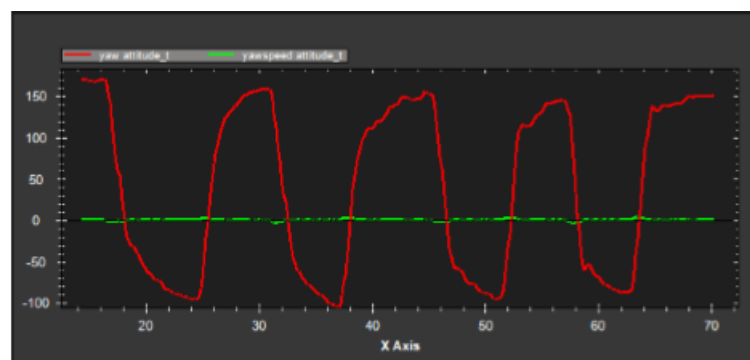


Figure 9.2 Yawing Stability with Disturbances

9.3 CONCLUSION

In conclusion, all the objectives of the project have been met. Through both theoretical and experimental studies of the aerodynamics and structural components of the UAV, it can be observed that most of the results concur and this provides useful information of VTOL UAVs. This uniquely spherical shaped UAV is definitely a class of its own as it has many characteristics which sets itself apart from most other UAVs currently in the market. Running only on a single propeller-motor configuration, the UAV is able to control and stabilise its yawing moment. During landing, the UAV rolls onto the ground until it comes to a standstill. It can then be piloted to an upright orientation before taking-off again. The Ground Station is able to provide Telemetry Information and status of UAV.

9.4 FUTURE SCOPE

Hover, climb vertically, and transit into translation flight, which is similar to that of a helicopter. Apart from that, this UAV boasts a new concept of take-off and landing, which is not commonly seen in most of the other UAVs is to be done in future.

FINAL PROTOTYPE



Figure – Final Prototype



Figure -Tethered final model during testing

APPENDIX - I

FLIGHT DYNAMIC EQUATION

MAV COORDINATE FRAMES

1. The inertial frame F^i
2. The vehicle frame F^v
3. The vehicle-1 frame F^{v1}

The transformation from F^v to F^{v1} is given by

$$p^{v1} = R_v^{v1}(\Psi)p^v$$

Where

$$R_v^{v1}(\Psi) = \begin{bmatrix} \cos \Psi & \sin \Psi & 0 \\ -\sin \Psi & \cos \Psi & 0 \\ 0 & 0 & 1 \end{bmatrix}$$

4. The vehicle-2 frame F^{v2}

The transformation from F^{v1} to F^{v2} is given by

$$p^{v2} = R_{v1}^{v2}(\theta)p^{v1}$$

Where

$$R_{v1}^{v2}(\theta) = \begin{bmatrix} \cos \theta & 0 & -\sin \theta \\ 0 & 1 & 0 \\ \sin \theta & 0 & \cos \theta \end{bmatrix}$$

5. The body frame F^b

The transformation from F^{v2} to F^b is given by

$$p^b = R_{v2}^b(\varphi)p^{v1\Phi}$$

Where

$$R_{v2}^b(\varphi) = \begin{bmatrix} 1 & 0 & 0 \\ 0 & \cos \varphi & \sin \varphi \\ 0 & -\sin \varphi & \cos \varphi \end{bmatrix}$$

The transformation from the vehicle frame to the body frame is given by

$$\begin{aligned} R_v^b(\varphi, \theta, \psi) &= R_{v2}^b(\varphi)R_{v1}^{v2}(\theta)R_v^{v1}(\psi) \\ &= \begin{bmatrix} 1 & 0 & 0 \\ 0 & \cos \varphi & \sin \varphi \\ 0 & -\sin \varphi & \cos \varphi \end{bmatrix} \begin{bmatrix} \cos \theta & 0 & -\sin \theta \\ 0 & 1 & 0 \\ \sin \theta & 0 & \cos \theta \end{bmatrix} \begin{bmatrix} \cos \psi & \sin \psi & 0 \\ -\sin \psi & \cos \psi & 0 \\ 0 & 0 & 1 \end{bmatrix} \\ &= \begin{bmatrix} \cos \theta \cos \psi & \cos \theta \sin \psi & -\sin \theta \\ \cos \varphi \sin \theta \cos \psi - \cos \varphi \sin \psi & \sin \varphi \sin \theta \cos \psi + \cos \varphi \cos \psi & \cos \varphi \sin \psi \\ \cos \varphi \sin \theta \sin \psi + \sin \varphi \cos \psi & \cos \varphi \sin \theta \cos \psi - \sin \varphi \cos \psi & \cos \varphi \cos \psi \end{bmatrix} \end{aligned}$$

6. The stability frame F^s

Since α is given by a left-handed rotation, the transformation from F^b to F^s is given by

$$p^s = R_b^s(\alpha)p^b$$

Where

$$R_b^s(\alpha) = \begin{bmatrix} \cos \alpha & 0 & \sin \alpha \\ 0 & 1 & 0 \\ \sin \alpha & 0 & \cos \alpha \end{bmatrix}$$

7. The wind frame F^w

The transformation from F^s to F^w is given by

$$p^w = R_s^w(\beta)p^s$$

Where

$$R_s^w(\beta) = \begin{bmatrix} \cos \beta & \sin \beta & 0 \\ -\sin \beta & \cos \beta & 0 \\ 0 & 0 & 1 \end{bmatrix}$$

The total transformation from the body frame to the wind frame is given by

$$\begin{aligned} R_b^w(\alpha, \beta) &= R_s^w(\beta) R_b^s(\alpha) \\ &= \begin{bmatrix} \cos \beta & \sin \beta & 0 \\ -\sin \beta & \cos \beta & 0 \\ 0 & 0 & 1 \end{bmatrix} \begin{bmatrix} \cos \alpha & 0 & \sin \alpha \\ 0 & 1 & 0 \\ \sin \alpha & 0 & \cos \alpha \end{bmatrix} \\ &= \begin{bmatrix} \sin \beta \cos \alpha & \sin \beta & \cos \beta \sin \alpha \\ -\sin \beta \cos \alpha & \cos \beta & -\sin \beta \sin \alpha \\ -\sin \alpha & 0 & \cos \alpha \end{bmatrix} \end{aligned}$$

KINEMATIC AND DYNAMICS

STATE VARIABLES

TABLE:

State variables for MAV equations of motion

Name	Description
p_n	Inertial north position of the MAV along \mathbf{i}^i in F^i
p_e	Inertial east position of the MAV along \mathbf{j}^i in F^i
p_d	Inertial down position of the MAV along \mathbf{k}^i in F^i
\mathbf{U}	Body frame velocity measured along \mathbf{i}^b in F^b
\mathbf{V}	Body frame velocity measured along \mathbf{j}^b in F^b
\mathbf{W}	Body frame velocity measured along \mathbf{k}^b in F^b
φ	Roll angle defined with respect to F^{v2}
θ	pitch angle defined with respect to F^{v1}
Ψ	yaw angle defined with respect to F^v
P	Roll rate measured along \mathbf{i}^b in F^b
Q	Pitch rate measured along \mathbf{j}^b in F^b
R	Yaw rate measured along \mathbf{k}^b in F^b

Kinematics:

The translational velocity of the UAV is commonly expressed in the velocity components along each of the axes in a fixed coordinate frame.

Relating the translational velocity and position requires differentiation and a rotational transformation.

$$\frac{d}{dt} \begin{pmatrix} p_n \\ p_e \\ p_d \end{pmatrix} = R_v^b \begin{pmatrix} u \\ v \\ w \end{pmatrix} = (R_v^b)^T \begin{pmatrix} u \\ v \\ w \end{pmatrix}$$

$$\begin{pmatrix} p_n \\ p_e \\ p_d \end{pmatrix} = \begin{bmatrix} c_\theta c_\psi & c_\phi s_\theta s_\psi - c_\phi s_\psi & c_\phi s_\theta c_\psi + s_\phi s_\psi \\ c_\theta s_\psi & s_\phi s_\theta s_\psi + c_\phi c_\psi & c_\phi s_\theta s_\psi - s_\phi c_\psi \\ -s_\theta & c_\theta s_\phi & c_\theta c_\phi \end{bmatrix} \begin{pmatrix} u \\ v \\ w \end{pmatrix}$$

$$\begin{pmatrix} p \\ q \\ r \end{pmatrix} = \begin{pmatrix} \varphi \\ 0 \\ 0 \end{pmatrix} + R_{v2}^b(\varphi) \begin{pmatrix} 0 \\ \theta \\ 0 \end{pmatrix} + R_{v2}^b(\varphi) R_{v1}^{v2}(\theta) \begin{pmatrix} 0 \\ 0 \\ \Psi \end{pmatrix}$$

$$= \begin{pmatrix} \varphi \\ 0 \\ 0 \end{pmatrix} + \begin{bmatrix} 1 & 0 & 0 \\ 0 & \cos \varphi & \sin \varphi \\ 0 & -\sin \varphi & \cos \varphi \end{bmatrix} \begin{pmatrix} 0 \\ \theta \\ 0 \end{pmatrix} +$$

$$\begin{bmatrix} 1 & 0 & 0 \\ 0 & \cos \varphi & \sin \varphi \\ 0 & -\sin \varphi & \cos \varphi \end{bmatrix} \begin{bmatrix} \cos \theta & 0 & -\sin \theta \\ 0 & 1 & 0 \\ \sin \theta & 0 & \cos \theta \end{bmatrix} \begin{pmatrix} 0 \\ 0 \\ \Psi \end{pmatrix}$$

$$= \begin{bmatrix} 1 & 0 & -\sin \theta \\ 0 & \cos \varphi & \sin \varphi \cos \theta \\ 0 & -\sin \varphi & \cos \varphi \cos \theta \end{bmatrix} \begin{pmatrix} \dot{\varphi} \\ \theta \\ \Psi \end{pmatrix}$$

Inversing the expression yields

$$\begin{pmatrix} \dot{\varphi} \\ \theta \\ \Psi \end{pmatrix} = \begin{bmatrix} 1 & \sin \varphi \tan \theta & \cos \varphi \tan \theta \\ 0 & \cos \varphi & -\sin \varphi \\ 0 & \sin \varphi \sec \theta & \cos \varphi \sec \theta \end{bmatrix} \begin{pmatrix} p \\ q \\ r \end{pmatrix}$$

This expresses the derivatives of the three angular position stated in terms of the angular positions Φ and θ and the body rates p , q and r .

RIGID BODY DYNAMICS

Applying newton's second law of motion

Expressing the $V_g^b = (u, v, w)^T$, the velocity of the vehicle with respect to the ground as expressed in the body frame.

1) TRANSLATIONAL MOTION

Newton's second law of motion applied to a body undergoing translational motion can be stated as

$$m \frac{dV_g}{dt_i} = f$$

Inertial frame to body frame

$$\frac{dV_g}{dt_i} = \frac{dV_g}{dt_b} + \omega_{\frac{b}{i}} \times V_g$$

$$m(\frac{dV_g}{dt_b} + \omega_{\frac{b}{i}} \times V_g) = f$$

expressing the forces and velocities in the body frame as

$$m(\frac{dV_g^b}{dt_b} + \omega_{\frac{b}{i}}^b \times V_g^b) = f^b$$

where

$$V_g^b = (u, v, w)^T$$

$$\omega_{\frac{b}{i}}^b = (p, q, r)^T$$

Since u , v and w are instantaneous projections of V_g^b onto the \mathbf{i}^b , \mathbf{j}^b and \mathbf{k}^b axes, it follows that

$$\frac{dV_g^b}{dt_b} = \begin{pmatrix} \dot{u} \\ \dot{v} \\ \dot{w} \end{pmatrix}$$

$$\begin{pmatrix} \dot{u} \\ \dot{v} \\ \dot{w} \end{pmatrix} = \begin{pmatrix} rv - qw \\ pw - ru \\ qu - pv \end{pmatrix} + \frac{1}{m} \begin{pmatrix} f_x \\ f_y \\ f_z \end{pmatrix}$$

2) ROTATIONAL MOTION

Newton's second law for rotational motion

$$\frac{dh}{dt_i} = m$$

Where h is the angular momentum in the vector form

The derivative of angular momentum taken in the inertial frame can be expressed as

$$\frac{dh}{dt_i} = \frac{dh}{dt_b} + \omega_b \times h = m$$

$$(\frac{d\mathbf{h}^b}{dt_b} + \omega_b \times \mathbf{h}^b) = \mathbf{m}^b$$

The angular momentum is defined as the product of the inertia matrix J and the angular velocity vector:

$$\mathbf{h}^b \triangleq J \omega_b \frac{\mathbf{b}}{I}$$

Where J is given by:

$$\begin{aligned} J &= \begin{pmatrix} \int (y^2 + z^2) dm & - \int xy dm & - \int xz dm \\ - \int xy dm & \int (x^2 + z^2) dm & - \int yz dm \\ - \int xz dm & - \int yz dm & \int (y^2 + x^2) dm \end{pmatrix} \\ &\triangleq \begin{pmatrix} J_x & -J_{xy} & -J_{xz} \\ -J_{xy} & J_y & -J_{yz} \\ -J_{xz} & -J_{yz} & J_z \end{pmatrix} \end{aligned}$$

FORCES AND MOMENTS

1) GRAVITATIONAL FORCES

$$f_g^v = \begin{pmatrix} 0 \\ 0 \\ mg \end{pmatrix}$$

$$f_g^v = R_v^b \begin{pmatrix} 0 \\ 0 \\ mg \end{pmatrix}$$

$$= \begin{pmatrix} -mg \sin\theta \\ mg \cos\theta \sin\phi \\ mg \cos\theta \cos\phi \end{pmatrix}$$

AERODYNAMIC FORCES AND MOMENTS

1) The lift, drag and moment are commonly expressed as

$$F_{lift} = \frac{1}{2} \rho V_a^2 S C_L$$

$$F_{drag} = \frac{1}{2} \rho V_a^2 S C_D$$

$$m = \frac{1}{2} \rho V_a^2 S c C_m$$

2) Longitudinal Aerodynamics

The Longitudinal Aerodynamics forces and moments cause motion in the body $\mathbf{i}^b - \mathbf{k}^b$ plane, known as the pitch plane

$$F_{lift} = \frac{1}{2} \rho V_a^2 S C_L(\alpha, q, \delta_e)$$

$$F_{drag} = \frac{1}{2} \rho V_a^2 S C_D(\alpha, q, \delta_e)$$

$$m = \frac{1}{2} \rho V_a^2 S c C_m(\alpha, q, \delta_e)$$

Taylor series expansion

$$F_{lift} = \frac{1}{2} \rho V_a^2 S \left[C_{L_0} + \frac{\partial C_L}{\partial \alpha} \alpha + \frac{\partial C_L}{\partial q} q + \frac{\partial C_L}{\partial \delta_e} \delta_e \right]$$

$$F_{lift} = \frac{1}{2} \rho V_a^2 S \left[C_{L_0} + C_{L_\alpha} \alpha + C_{L_q} \frac{c}{2V_a} q + C_{L_{\delta_e}} \delta_e \right]$$

Similarly

$$F_{drag} = \frac{1}{2} \rho V_a^2 S \left[C_{D_0} + C_{D_\alpha} \alpha + C_{D_q} \frac{c}{2V_a} q + C_{D_{\delta_e}} \delta_e \right]$$

$$m = \frac{1}{2} \rho V_a^2 S c \left[C_{m_0} + C_{m_\alpha} \alpha + C_{m_q} \frac{c}{2V_a} q + C_{m_{\delta_e}} \delta_e \right]$$

The linear lift coefficient

$$C_{L_\alpha} = \frac{\pi A R}{1 + \sqrt{1 + \left(\frac{AR}{2}\right)^2}}$$

Combining the parasitic drag and the induced drag, we get

$$C_D(\alpha) = C_{D_p} + \frac{(C_{L_0} + C_{L_\alpha} \alpha)^2}{\pi e A R}$$

3) Lateral Aerodynamics

The lateral aerodynamic force and moments cause translational motion in the lateral direction along the \mathbf{j}^b axis as well as rotational motions in roll and yaw that will result in directional changes in the flight path of the aerial vehicle.

$$f_y = \frac{1}{2} \rho V_a^2 S C_y(\beta, p, r, \delta_a, \delta_r)$$

$$l = \frac{1}{2} \rho V_a^2 S b C_l(\beta, p, r, \delta_a, \delta_r)$$

$$n = \frac{1}{2} \rho V_a^2 S b C_n(\beta, p, r, \delta_a, \delta_r)$$

Linear relationships for lateral force, roll moment and yaw moment are given by

$$f_y = \frac{1}{2} \rho V_a^2 S \left[C_{y_0} + C_{y_\beta} \beta + C_{y_p} \frac{b}{2V_a} p + C_{y_r} \frac{b}{2V_a} r + C_{y_{\delta_a}} \delta_a + C_{y_{\delta_r}} \delta_r \right]$$

Similarly

$$l = \frac{1}{2} \rho V_a^2 S b \left[C_{l_0} + C_{l_\beta} \beta + C_{l_p} \frac{b}{2V_a} p + C_{l_r} \frac{b}{2V_a} r + C_{l_{\delta_a}} \delta_a + C_{l_{\delta_r}} \delta_r \right]$$

$$n = \frac{1}{2} \rho V_a^2 S b \left[C_{n_0} + C_{n_\beta} \beta + C_{n_p} \frac{b}{2V_a} p + C_{n_r} \frac{b}{2V_a} r + C_{n_{\delta_a}} \delta_a + C_{n_{\delta_r}} \delta_r \right]$$

APPENDIX – II

FLIGHT COMPUTER CODE

```
#include<Servo.h>
#include <Wire.h>
#include <Adafruit_Sensor.h>
#include <Adafruit_BNO055.h>
#include <utility/imumaths.h>
#define BNO055_SAMPLERATE_DELAY_MS (10)
#define BEEP 11
#define HWS Serial
// **** CDH
String s1, s2, s3, s4;
char Str1[3] = "X";
char Str2[3] = "Y";
char Str3[3] = "Z";
char Str4[3] = "B";
int Buttons; //Digital Buttons
int x = 4095;
int y = 4095;
int z = 4095;
int btn = 0;
int la = 4095;
int lo = 4095;
int al = 4095;

int X, Y, Z; //Analog
boolean buttons[10];
boolean flag = 0;
```

```

//*****
Adafruit_BNO055 bno = Adafruit_BNO055(55);
boolean state;
Servo F1, F2, F3, F4, R1, R2, R3, R4, ESC;
short rcPin[] = { 13, 14, 15, 16};

void setup()
{
    Serial.begin(115200);
    ESC.attach(6, 900, 2200);
    ESC.writeMicroseconds(900);
    R1.attach(2, 750, 2200); //1450
    R2.attach(4, 750, 2200); //1360
    R3.attach(5, 750, 2200); //1490
    R4.attach(3, 750, 2200); //1430 -550 to + 550
    F1.attach(20, 750, 2200);
    F2.attach(21, 750, 2200);
    F3.attach(22, 750, 2200);
    F4.attach(23, 750, 2200);
    R1.writeMicroseconds(1450);
    R2.writeMicroseconds(1360);
    R3.writeMicroseconds(1490);
    R4.writeMicroseconds(1430);

    F1.writeMicroseconds(1250); //1250
    F2.writeMicroseconds(1350); //1350
    F3.writeMicroseconds(1370); //1350
    F4.writeMicroseconds(1280); //1280
    delay(100);
}

```

```

pinMode(13, INPUT);
pinMode(14, INPUT);
pinMode(15, INPUT);
pinMode(16, INPUT);

pinMode(BEEP, OUTPUT);
/* Initialise the sensor */
if (!bno.begin())
{
    while (!bno.begin())
    {
        digitalWrite(BEEP, state);
        state = !state;
        delay(500);
    }
    digitalWrite(BEEP, 1);
    delay(200);
    digitalWrite(BEEP, 0);
}
}

uint16_t ch[4], chMax[] = {1800, 1800, 1800, 1800}, chMin[] = {1100, 1100, 1100,
1100};
uint16_t SPD = 900;

int roll, pitch, yaw;
float PIDroll, I_roll, D_roll, p_roll, rkp = 24.02, rki, rkd = 0;
float PIDpitch, I_pitch, D_pitch, p_pitch, pkp = 24.02, pki, pkd = 0;
float PIDyaw, I_yaw, D_yaw, p_yaw, ykp = 50.2, yki = 0.2, ykd = 3;
float PID, P, I, D, kp, ki, kd, p_P;

```

```

uint32_t t, p_t, dt, slp;
int a, b, c;
int np, nr;
boolean rcflag;

void loop()
{
    t = millis();
    dt = t - p_t;
    p_t = t; //time

    uint8_t sys, gyro, accel, mag = 0;
    bno.getCalibration(&sys, &gyro, &accel, &mag);
    imu::Vector<3> euler = bno.getVector(Adafruit_BNO055::VECTOR_EULER);
    imu::Vector<3> GY =
    bno.getVector(Adafruit_BNO055::VECTOR_GYROSCOPE);

    if (1)
    {
        x = (euler.z() + 180); //roll
        y = (euler.y() + 180); //pitch
        z = (euler.x() + 180); //yaw

        digitalWrite(BEEP, 0);
        roll = euler.z(); // roll
        pitch = euler.y(); // pitch
        yaw = euler.x() - 180;
        P = GY.z();

    }
    else
    {

```

```

ESC.writeMicroseconds(900);

state = !state;

digitalWrite(BEEP, state);

}

for (short i = 0; i < 4; i++)

{

ch[i] = pulseIn(rcPin[i], HIGH, 20000);

if (ch[i] > 800)

{

chMin[i] = chMin[i] > ch[i] ? ch[i] : chMin[i];

chMax[i] = chMax[i] < ch[i] ? ch[i] : chMax[i];

}

}

if (ch[0] > 0)

{

SPD = map(ch[2], chMin[2], chMax[2], 900, 2200);

rcflag = 1;

}

else

{

SPD = 900;

//rcflag = 0;

}

I += P;

D = P - p_P;

```

```

PID = P * 85 + I * 0 * dt + 10 * D / dt;
p_P = P;

D_roll = roll - p_roll;
I_roll += roll;
PIDroll = 30 * roll + rki * I_roll + 0 * D_roll / dt;
p_roll = roll;

```

```

D_pitch = pitch - p_pitch;
I_pitch += pitch;
PIDpitch = 30 * pitch + pki * I_pitch + 0 * D_pitch / dt;
p_pitch = pitch;

```

```

D_yaw = yaw - p_yaw;
I_yaw += yaw;
PIDyaw = 0 * yaw + 0 * I_yaw + 0 * D_yaw / dt;
p_yaw = yaw;

```

```

PIDyaw = PIDyaw > 200 ? 200 : PIDyaw;
PIDyaw = PIDyaw < -200 ? -200 : PIDyaw;

```

```

np = roll * cos(0.7854) - pitch * cos(0.7854);
nr = roll * sin(0.7854) + pitch * sin(0.7854);

```

```

float PIDnroll = 20 * nr;
float PIDnpitch = 20 * np;

a = PID;
b = PIDpitch ;

```

```

c = PIDroll ;

a = a > 600 ? 600 : a;

a = a < -600 ? -600 : a;

b = b > 600 ? 600 : b;

b = b < -600 ? -600 : b;

int zang = map(ch[0], chMin[0], chMax[0], -400, 400);

int yang = map(ch[1], chMin[1], chMax[1], -400, 400);

int xang = map(ch[3], chMin[3], chMax[3], -400, 400);

int p = a - PIDyaw * 0;

// R1.writeMicroseconds(1450 - PIDpitch * 0 + p + xang);

// R3.writeMicroseconds(1490 + PIDpitch * 0 + p - xang);

// R2.writeMicroseconds(1360 + PIDroll * 0 + p + yang);

// R4.writeMicroseconds(1430 - PIDroll + p - yang);

R1.writeMicroseconds(1450 + a);

R3.writeMicroseconds(1490 + a);

R2.writeMicroseconds(1360 + a);

R4.writeMicroseconds(1430 + a);

// R1.writeMicroseconds(1450 - PIDnroll + p + xang);

// R3.writeMicroseconds(1490 + PIDnroll + p - xang);

// R2.writeMicroseconds(1360 + PIDnpitch + p + yang);

// R4.writeMicroseconds(1430 - PIDnpitch + p - yang);

//


F1.writeMicroseconds(1250 + b); //1250

F2.writeMicroseconds(1350 - b); //1350

F3.writeMicroseconds(1370 - c); //1350

```

```
F4.writeMicroseconds(1280 + c); //1280
```

```
ESC.writeMicroseconds(SPD);
```

```
// Serial.print(b); Serial.print(" c");  
// Serial.print(c); Serial.print(" ");  
// Serial.print(roll); Serial.print(" ");  
// Serial.print(pitch); Serial.print(" ");  
//  
if ((millis() - slp) > 100)  
{  
    sendPacket();  
    slp = millis();  
}  
// Serial.println();
```

```
}
```

```
void printRC()  
{  
    Serial.print(ch[0]); Serial.print(" ");  
    Serial.print(ch[1]); Serial.print(" ");  
    Serial.print(ch[2]); Serial.print(" ");  
    Serial.print(ch[3]); Serial.print(" | ");  
    Serial.print(chMax[0]); Serial.print(" ");  
    Serial.print(chMax[1]); Serial.print(" ");  
    Serial.print(chMax[2]); Serial.print(" ");  
    Serial.print(chMax[3]); Serial.print(" | ");
```

```
Serial.print(chMin[0]); Serial.print(" ");
Serial.print(chMin[1]); Serial.print(" ");
Serial.print(chMin[2]); Serial.print(" ");
Serial.print(chMin[3]);;
}
```

LIST OF FABRICATORS

- i. Aluminium spars fabrication
Name of industry – SYSPRO EDM
Address - No: mathiyazhagan nagar, 17-56, Amman Koil St, Elango Nagar, Padi, Chennai, Tamil Nadu 600050
- ii. Core body – ABS-M30
Name of industry – SRM RPT LAB (3D printing)
Address - Mechanical Block-A, Department of Mechanical engineering, Srm University, kattankulathur, Chennai
- iii. Control surfaces – Balsa
Material Purchased – Sree Sai Aerotech Innovations
Address - New No. 21, Old No. 12, First Floor, Teachers Colony, Adyar, Chennai, Tamil Nadu 600020

REFERENCES

RAYMER, D. P. 1991. *Aircraft Design: A conceptual Approach*, Wright-Patterson Air Force Base, Ohio, American Institute of Aeronautics and Astronautics, Inc.

ROSKAM, J. 1985. *Preliminary Sizing of Airplanes*, DARcorporation.
<http://whatis.techtarget.com/definition/ampere-hour-Ah-or-amp-hour>
raphael.mit.edu/xfoil/

<http://www.mh-aerotools.de/airfoils/images/prop1.gif>

http://www.hobbyking.com/hobbyking/store/__37798__Turnigy_D3548_4_1100KV_Brushless_Outrunner_Motor_US_Warehouse_.html

http://www.hobbyking.com/hobbyking/store/__80506__Aerostar_50A_Electronic_Speed_Controller_with_5A_BEC_2_6S_.html

<http://www.makeitfrom.com/>

<http://www.matweb.com/>

<http://www.matdat.com/MainMenuItem.aspx?idM=2&subM=41>

<http://www.matbase.com/>

http://www.hobbyking.com/hobbyking/store/uh_viewitem.asp?idproduct=8932

<https://www.pjrc.com/teensy/teensy31.html>

<https://www.tindie.com/products/onehorse/bmx-055-9-axis-motion-sensor-add-on-for-teensy-31/>

<https://www.tindie.com/products/onehorse/bno-055-9-axis-motion-sensor-with-hardware-sensor-fusion/>